Journal of
Marine Science and Engineering

MDPI

Article

The Environmental Niche of the Light Purse Seine Fleet in the Northwest Pacific Ocean Based on Automatic Identification System Data

Shenglong Yang [1,3,*], Lijun Wan [1,3,4,†], Linlin Yu [1,3,5], Jiashu Shi [1,3,4], Weifeng Zhou [1,3], Shengmao Zhang [1,2,3], Fei Wang [1,3], Zuli Wu [1,3], Yang Dai [1,3], Keji Jiang [1,3] and Wei Fan [1,3,*]

1 Key Laboratory of Fisheries Remote Sensing, Ministry of Agriculture and Rural Affairs, East China Sea Fisheries Research Institute, Chinese Academy of Fishery Sciences, Shanghai 200090, China; fuxiao3614@163.com (L.W.); evelyn_lovesea@hotmail.com (L.Y.); sjsmq20200701@gmail.com (J.S.); zhou_wf@hotmail.com (W.Z.); zhangsm@ecsf.ac.cn (S.Z.); essiwf@163.com (F.W.); wuzl@ecsf.ac.cn (Z.W.); daiyangbox@163.com (Y.D.); jiangkj@ecsf.ac.cn (K.J.)
2 Laoshan Laboratory, Qingdao 266237, China
3 Key and Open Laboratory of Remote Sensing Information Technology in Fishing Resource, Chinese Academy of Fishery Sciences, Shanghai 200090, China
4 School of Navigation and Naval Architecture, Dalian Ocean University, Dalian 116023, China
5 College of Information, Shanghai Ocean University, Shanghai 201306, China
* Correspondence: ysl6782195@126.com (S.Y.); fanw@ecsf.ac.cn (W.F.); Tel.: +86-1376-4672-421 (S.Y.)
† The author contributed to the work equally and should be regarded as co-first authors.

Abstract: Ecosystem-based fisheries management requires high-precision fisheries information to provide relevant data for natural resource management, assessment, and marine spatial planning. This study utilizes Automatic Identification System (AIS) data from light purse seine vessels from the Chinese mainland that were collected from May to November between 2020 and 2022, along with the corresponding environmental data. By applying boosted regression trees (BRTs) and generalized additive models (GAMs), this study establishes nonlinear relationships between fishing intensity and predictor variables and explores the ecological and environmental drivers behind the spatial distribution of light purse seine vessels from the Chinese mainland in the Northwest Pacific. This research identifies the key influencing factors and reveals significant seasonal preferences for different marine environments in various months, with chlorophyll-a being the primary influencing factor. The predicted fishing effort closely resembles observed data, providing valuable information to support fisheries resource management and planning.

Keywords: Northwest Pacific Ocean; light purse seine vessels; AIS; GAM; BRT

Citation: Yang, S.; Wan, L.; Yu, L.; Shi, J.; Zhou, W.; Zhang, S.; Wang, F.; Wu, Z.; Dai, Y.; Jiang, K.; et al. The Environmental Niche of the Light Purse Seine Fleet in the Northwest Pacific Ocean Based on Automatic Identification System Data. *J. Mar. Sci. Eng.* **2024**, *12*, 1944. https://doi.org/10.3390/jmse12111944

Academic Editor: Antonello Sala

Received: 2 October 2024
Revised: 23 October 2024
Accepted: 29 October 2024
Published: 31 October 2024

1. Introduction

Chub mackerel (*Scomber japonicus*) is an important economic species in marine fishery and one of the most commercially valuable fish in the world. It is an important source of food with high nutritional value and contributes significantly to reducing hunger and addressing malnutrition [1,2]. However, the increasing demand for seafood over the past few decades has put significant pressure on marine ecosystems. In this context, the scientific monitoring and regulation of fishery resources and regional fishing intensities are necessary. Domestic and international researchers have conducted many relevant studies, with most research based on analyses of commercial fishing data. Regional data on chub mackerel are relatively complete, but they have low spatial and temporal resolutions. Although commercial fishing data from various countries are highly accurate, they are often incomplete and may contain some errors. These data are of limited value in assessing regional fishing intensities and the distribution of fishery resources, which constrains research on the mechanisms of the spatiotemporal changes in regional fishing activities.

To better achieve ecosystem-based fisheries management, it is essential to understand the impacts of fishing activities, such as habitat destruction or changes to ecological communities associated with fishing activities. The advent of the Automatic Identification System (AIS) has provided high spatiotemporal resolution trajectory data for fishing vessel positioning. It is widely used in monitoring and managing marine fishing activities and assessing ecological pressures, making it an important tool for quantitative research on marine fisheries. However, the extracted fishing intensity information can only reflect historical fishing vessel activities and cannot reveal future fishing vessel distributions and trends. Additionally, owing to deliberate AIS shutdowns or transmission issues, there is a significant amount of invisible fishing intensity globally [3,4], posing serious challenges to the objective understanding of fishing activities.

Soykan et al. (2014) developed a BRT model for predicting fishing efforts based on environmental and spatial variables. The model accurately predicted fishing effort one year later, indicating that fishing effort can be forecasted using a model [5]. Setiawati et al. (2015) used a statistical method combining Generalized Additive Models (GAMs) and Geographic Information Systems (GISs) to analyze the relationship between daily catch data and satellite data. The results of the GAM showed that environmental variables strongly influence the catch amount of bigeye tuna [6]. Hashimoto et al. (2019) derived the CPUE of chub mackerel using both the GLM and GAM [7]. Similarly, Shi et al. (2019) also estimated the CPUE of chub mackerel using a GLM and GAM, with better results obtained using the GAM [8]. Therefore, the potential distribution of future fishing efforts under different climate scenarios can be analyzed and discussed, providing support for long-term management planning in fisheries resource management.

Research on the environmental niches of fishing activities has shown that the distribution of offshore fishing intensities can be explained and modeled on the basis of marine environmental variables [9–12]. Studies indicate that results based on AIS data are similar to those based on commercial fishing data, suggesting that marine environments indirectly influence fishing operations by directly affecting fishery resources. Analyzing and discussing the potential distribution of future fishing efforts under different climate scenarios can fill gaps in AIS data, providing high-precision data support for fishery resource management and planning.

In the Northwest Pacific, the majority of the chub mackerel catch comes from light purse seine vessels. Wan et al. (2024) analyzed the spatial distributions of these vessels in the Northwest Pacific but did not discuss the factors driving their spatial operations [13]. This study extracts information on the fishing efforts of light purse seine vessels from the Chinese mainland in the Northwest Pacific and establishes a nonlinear relationship between fishing intensity and environmental variables. While the generalized additive model (GAM) has been widely used in studies of chub mackerel [7,8], studies using the BRT model for chub mackerel are still relatively rare. This study explores the ecological and environmental drivers of the spatial distribution of these vessels and predicts the spatiotemporal distribution of fishing intensity, providing data support for the management of chub mackerel fisheries.

2. Materials and Methods

2.1. Study Region

Figure 1 reports that from 2020 to 2022, Chinese mainland light purse seine vessels were distributed primarily in the Northwest Pacific between 35° and 50° N and between 140° and 160° E. Therefore, this area was selected as the study region for this paper.

2.2. Spatial and Temporal Patterns

AIS data were sourced from the SPIRE satellite. We obtained information on light purse seine vessels in the Northwest Pacific Ocean from the Light Purse Seine Vessels Science and Technology Group of the Chinese mainland. The fishing intensity was defined as the fishing effort per unit area and unit time [13]. To match the environmental data, the spatial resolution of the fishing effort dataset was adjusted to 0.25° × 0.25°, with a monthly temporal resolution.

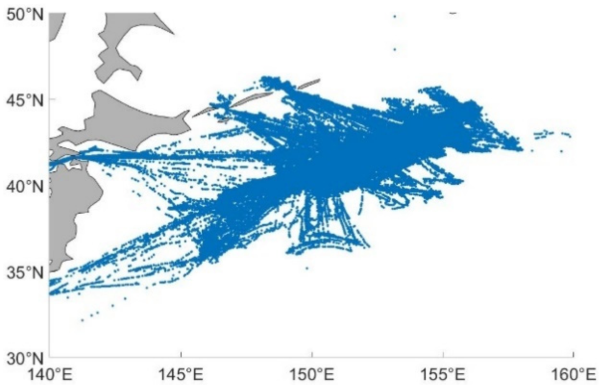

Figure 1. The Chinese mainland light purse seine vessel track map from 2020 to 2022.

We first mapped the spatial distribution of the total fishing effort for Chinese mainland light purse seine vessels in the Northwest Pacific. The effort-by-cell data were averaged across the years from 2020 to 2022. To understand the spatial patterns of these vessels, we plotted the density curve of fishing effort across spatial cells. To illustrate the spatial concentration of fishing effort, a Q-Q diagram was designed with the cumulative quantile of fishing effort plotted against the cumulative quantile of fishing areas.

A similar analysis was conducted to examine the temporal patterns of fishing efforts. From 2020 to 2022, the fishing efforts were aggregated by day, and the general time trend was illustrated using a "LOESS" smoothing curve to reduce the impact of daily fluctuations. LOESS (locally weighted regression) is a non-parametric method used for local regression analysis. It works by dividing the sample data into small intervals, fitting a polynomial within each interval, and repeating this process to obtain weighted regression curves for different intervals. These curves are then connected at their centers to form a complete regression curve. We also used density curves of fishing effort per day to examine the temporal pattern and created a Q-Q diagram to indicate the temporal concentration of fishing effort.

2.3. Environmental Variables

This study revealed that the habitat of chub mackerel is influenced by environmental variables such as temperature, sea surface height, salinity, chlorophyll, dissolved oxygen, and primary productivity [14–16]. The vertical spatial distribution of chub mackerel is also related to subsurface environmental factors.

The vertical distribution of chub mackerel is an important characteristic. In the Northwest Pacific, chub mackerel occupy depths of 0–300 m, with the average depth during the day being deeper than that observed at night during the feeding season [17]. Therefore, we selected environmental variables at depths of 0 m, 100 m, 200 m, and 300 m (Table A1). We utilized marine remote sensing environmental data that were downloaded from the Copernicus Marine Environment Monitoring Service (CMEMS) (https://resources.marine.copernicus.eu/?option=com_csw&task=results?option=com_csw&task=results, accessed on 9 October 2023). The temporal resolution of the environmental data on this website is available in both daily and monthly formats. Within the range of 35° to 50° N and 140° to 160° E, using daily resolution for training results in relatively small amounts of daily fishing effort data, which could negatively impact model performance. On the other hand, training with yearly resolution would fail to capture the seasonal migration patterns of chub mackerel. Therefore, using monthly intervals is more appropriate. Additionally, the spatial resolution of physics variables is fixed at 0.083° × 0.083°, while biogeochemistry variables have a resolution of 0.25° × 0.25°. As a result, the spatial resolution of the environmental data is standardized to 0.25° × 0.25°.

A method for calculating the SST front (*sstf*) was proposed by Belkin et al. (2009) [18]. This method uses satellite images of chlorophyll and sea surface temperature to detect ocean fronts. The formula for calculating *sstf* is as follows

$$sstf = \sqrt{(Gx^2 + Gy^2)} \tag{1}$$

where Gx and Gy are computed using the Sobel operator consisting of two 3×3 convolution masks or kernels: Gx = [− 1 0 + 1; − 2 0 + 2; − 1 0 + 1] and Gy = [+ 1 + 2 + 1; 0 0 0; − 1 −2 − 1], respectively.

The formula for calculating EKE is as follows [19]

$$EKE = \frac{1}{2}\left(u^2 + v^2\right) \tag{2}$$

where v and u are the meridional and zonal components of the geostrophic currents, respectively.

2.4. Multicollinearity Inspection

For a multiple regression model, severe multicollinearity among independent variables can reduce the model's accuracy and stability. The variance inflation factor (VIF) method is commonly used to detect multicollinearity issues within a regression model. Generally, if each variable in a regression model has a VIF between 1 and 5, the model does not have serious multicollinearity concerns [20]. We used the lm function in R to build a multiple linear model with the variables in Table A1 as independent variables and fishing efforts as the dependent variable; this model was used to detect whether there is multicollinearity among the environmental variables. Then, we used the vif function from the car package in R to calculate the VIF value for each environmental variables in the fitted model. Finally, the environmental variables were selected based on the linear correlation coefficients between each pair of variables and the VIF value for each variable, ensuring that the VIF values of each variable were between 1 and 5. The remaining variables were used for analysis in this paper.

2.5. BRT Model

The boosted regression trees (BRTs) model is an ensemble learning method based on decision trees [21], that is used for explanation and prediction in ecological statistical models. The BRT model is particularly effective for interpreting and predicting certain characteristics, such as nonlinear variables and interactions among variables. The BRT model combines the strengths of tree-based models, handles different types of predictor variables, and allows for missing data. This method does not require prior data transformation or outlier removal, can fit complex nonlinear relationships, and can automatically manage interactions among predictor variables. The process of fitting multiple trees in the BRT model compensates for the weak predictive ability of a single-tree model, providing stronger predictive capabilities than many traditional modeling methods. It can address a wide range of practical issues in model fitting [22]. BRT's low generalization error can also be attributed to its lower proneness to overfitting.

The BRT model was constructed using the formula below [23]:

$$f_M(X) = \sum_{m=1}^{M} T_m(X, \gamma_m) \tag{3}$$

where X represents the environmental variables from Table A1 used as predictor variables, T_m represents the regression tree with index M, and γ_m represents its parameters, indicating the split points of the tree and the values assigned to each leaf node. The learning process of decision tree T_m is essentially the same process as solving for γ [24]. The BRT model was constructed using the gbm.step function from the dismo package in R (version 4.2.2).

In this paper, we aim to use BRT to predict potential fishing effort locations based on environmental data. Therefore, we use the presence or absence of fishing effort at a given location (a 0.1° × 0.1° grid) as the dependent variable to construct the BRT model. Grids with FE were assigned a value of "1", while those without FE were given a value of "0". The predictor variables included longitude, latitude, distance from the shore, and various environmental factors. The BRT model was applied using a Bernoulli distribution.

The dataset for each month was split into 10 parts to create cross-validation sets to improve the accuracy and stability of the BRT model. Nine of these parts were used for training, while one was reserved for validation. This process resulted in the creation of 10 BRT models per month.

The BRT model involves three key parameters: the learning rate (lr), tree complexity (tc), and bagging fraction. lr plays a crucial role in determining the model's growth and helps prevent overfitting [24]. It is typically advised to select an lr value that allows the model to develop at least 1000 trees [22]. Tree complexity (tc) refers to the number of nodes in each tree, representing the degree of interaction between the predictor variables within the model [21]. The bagging fraction represents the proportion of data used in each step of building the model, and this value is typically set between 0.5 and 0.75 [22]. According to Elith et al. (2008), it is often a better choice to combine an increased tc and a reduced lr [22]. Based on these insights, we set the learning rate (lr) at four levels: 0.05, 0.01, 0.005, and 0.001. Tree complexity (tc) was assigned values of 5, 6, 7, and 8, while the bagging fraction remained fixed at 0.5. The model assumes a Bernoulli distribution for its distributional hypothesis. The optimal parameters were determined using prediction deviation. We built trees with different parameter settings to obtain the most appropriate model parameters for each month, with a maximum node limit of 20,000 for each month and plotted the fitting curve for each model.

2.6. GAM

In this study, we employed the GAM as a reference for comparison with the BRT model. We built the GAM using the gam function from the mgcv package in R. The process of constructing the GAM is comparable to that of the BRT model. The model assumes a Bernoulli distribution for its distributional hypothesis, with the initial variable selection consistent with the BRT model.

2.7. Parameters for Evaluating the Models

In this study, we evaluated the accuracy and stability of the BRT and GAM using explained deviance and the area under the receiver operating characteristic (ROC) curve (AUC). The AUC serves as a performance metric to assess model quality, with values above 0.75 generally indicating that the model is useful [25]. The AUC values for the models were calculated using the ROCR package in R. Explained deviance is another commonly used metric for model evaluation, with higher values closer to 100%, indicating better model performance [26]. The F1 score, defined as the harmonic mean of the precision and recall, ranges from 0 to 1, with higher values being preferable. The kappa score, which measures consistency and classification performance, is derived from the confusion matrix and ranges from −1 to 1, with values generally above 0 indicating agreement. It is mainly affected by prevalence or the proportion of positive cases within a sample [27]. For each month, we choose the BRT models with the highest AUC value. The GAM was used as a reference for the BRT model, with as many variables selected as possible and all variables having a significant impact. Finally, we performed a global sensitivity analysis on the BRT model using Sobol indices. The goal of global sensitivity analysis is to assess the contribution of each input variable to the variance of the model output, considering the variation in the variables across the entire input space rather than just at specific points or intervals. Sobol indices decompose the model output variance, calculating the direct contribution of each input variable (first-order Sobol indices) and the interactions between variables (total Sobol indices).

3. Results

3.1. Spatial Distribution Patterns

Figure 2A shows the distribution of the average fishing effort by Chinese mainland light purse seine vessels from 2020 to 2022. Most fishing activities are concentrated near the boundary line of the exclusive economic zone (EEZ), with fishing efforts increasing as the proximity to the EEZ boundary line decreases. Fishing effort across spatial units generally follows log-normal distributions (Figure 2B), with a mean of 58.6 h and a standard deviation of 97.3 h. As shown in Figure 2C, the spatial distributions of fishing efforts are highly concentrated, with 15% of the areas contributing 80% of the total fishing effort.

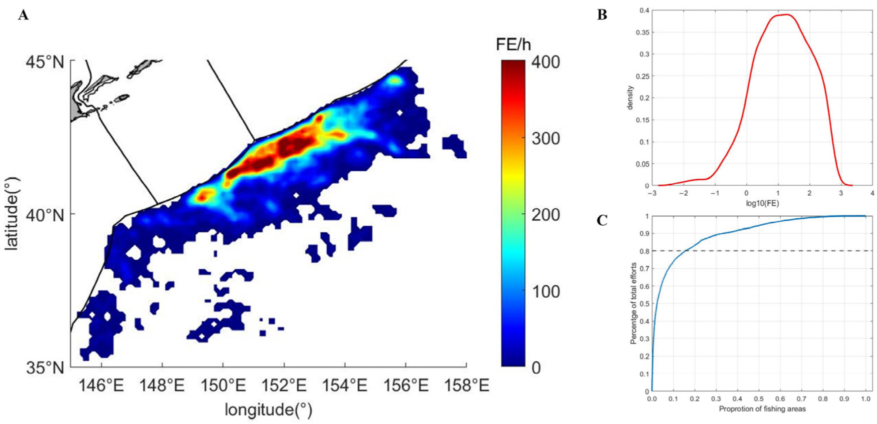

Figure 2. (**A**) Spatial distribution map of the average fishing effort by Chinese mainland light purse seine vessels from 2020 to 2022. (**B**) Density curve of histograms of the average fishing effort from 2020 to 2022. (**C**) Q-Q diagram showing the cumulative quantile of fishing effort against the corresponding cumulative quantile of fishing areas.

3.2. Temporal Distribution Patterns

Figure 3A shows the temporal distribution of daily fishing efforts by Chinese mainland light purse seine vessels from 2020 to 2022. The temporal distribution of fishing efforts exhibited a clear seasonal pattern, with most fishing activities occurring between May and November each year. The density curve of daily fishing effort is less regular than the spatial curve (Figure 3B) with an average of 136.8 h and a maximum of 271.1 h. As shown in Figure 3C, the temporal distribution of fishing effort is relatively even, with 80% of the total fishing effort carried out 70% of the time.

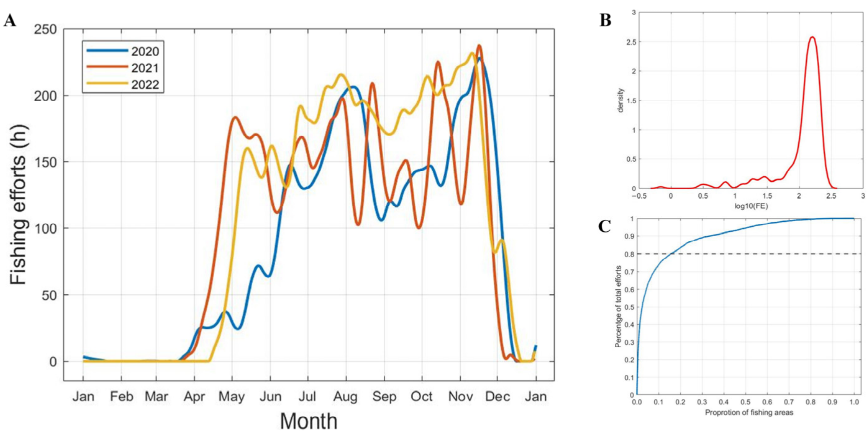

Figure 3. (**A**) Daily fishing effort distribution curve of Chinese mainland light purse seine vessels from 2020 to 2022. (**B**) Density curve of histograms of the average daily fishing effort from 2020 to 2022. (**C**) Q-Q diagram showing the cumulative quantile of fishing effort against the corresponding cumulative percentage of days.

3.3. Multicollinearity of the Model

We built a multiple linear regression model using the FE data and environmental variables and then calculated the VIF values for each environmental variable to assess multicollinearity. As shown in Figure 4A, except for sea surface temperature (T0), the VIF values for temperatures at other depths were very high. The highest VIF value was 495.32 for the temperature at a depth of 200 m (T200), whereas the lowest was 1.03 for the northward velocity (v) (Figure 4A). We then calculated the correlation coefficients between variables and removed some based on their VIF values. After certain variables were removed, the VIF values for all remaining variables were less than 5. The highest VIF value was 4.42 for the temperature at 300 m depth (T300), and the lowest was 1.02 for the northward velocity (v) (Figure 4B). As depicted in Figure 5, the absolute values of the linear correlation coefficients among the remaining variables were all below 0.8. This suggests that there were no significant multicollinearity issues among the remaining variables.

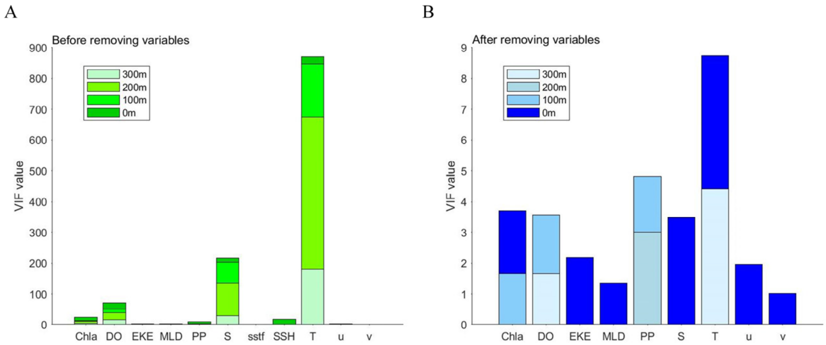

Figure 4. (**A**) VIF values for each environmental variable before removing variables. (**B**) VIF values for each environmental variable after removing variables.

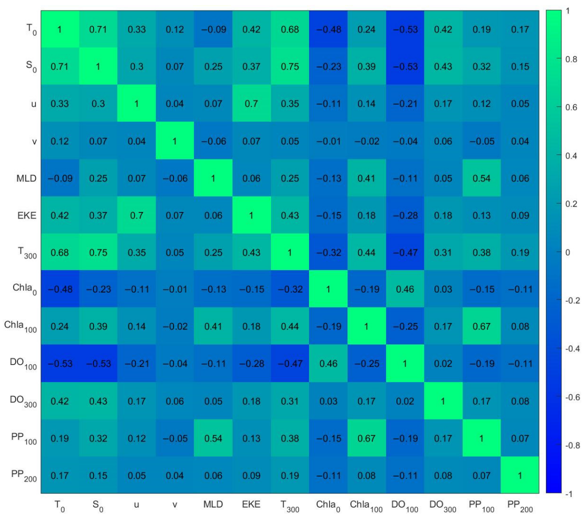

Figure 5. The linear correlation coefficients among the remaining variables after removing variables.

3.4. Parameter Settings for the BRT Model

As illustrated in Figure A1a–g, the BRT model's fitting time for each month is significantly extended when the lr is set to 0.001. Additionally, the fitted curve exhibits a continuous downward trend, suggesting that the predictive deviation has not yet reached its minimum. We selected the optimal parameters for each month based on the criterion of the model reaching the lowest predictive deviation as quickly as possible. The parameters selected each month are listed in Table 1.

Table 1. The parameters selected for the BRT model from May to November.

Month	Learning Rate	Tree Complexity
May	0.01	7
June	0.01	7
July	0.01	7
August	0.01	8
September	0.01	8
October	0.01	8
November	0.01	8

3.5. Performance of the BRT Model and the GAM

The deviance explained by the BRT model was greater than 0.5 for each month, with the lowest deviance explained (in May) exceeding 0.55 (Figure 6A). The average AUCs for each month were consistently above 0.94, with the lowest AUC value (in July) also exceeding 0.94 (Figure 6B). These results indicate that the BRT model we constructed possesses high stability and accuracy, making it suitable for further analysis. The best BRT model for each month is listed in the table. The deviance explained and AUC values each month exceeded 70% and 0.9, respectively, as shown in Table 2.

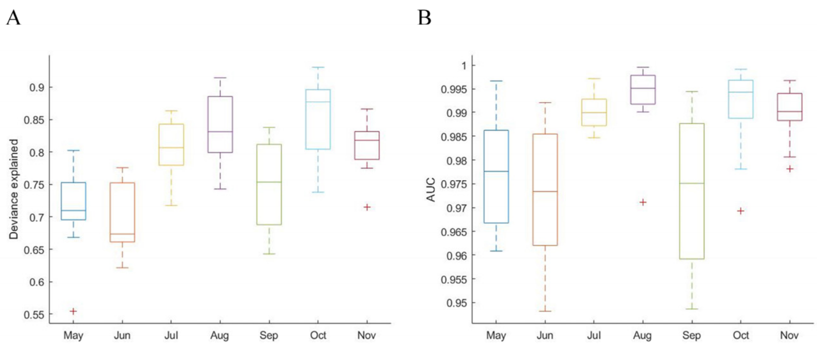

Figure 6. (**A**) Boxplot of the average deviance explained by the BRT model for each month; (**B**) Boxplot of the average AUC values of the BRT model for each month.

Table 2. The prediction results of the optimal BRT model and GAM for each month.

	BRT				GAM			
Month	Deviance Explained/%	F1 Score	AUC	Kappa	Deviance Explained/%	F1 Score	AUC	Kappa
May	79.3	0.783	0.996	0.779	76.3	0.497	0.977	0.482
June	75.5	0.720	0.991	0.712	74.9	0.547	0.971	0.527
July	82.6	0.807	0.995	0.803	84.5	0.628	0.987	0.617
August	91.3	0.984	0.999	0.984	90.3	0.746	0.992	0.739
September	80.9	0.860	0.995	0.856	79.4	0.555	0.976	0.539
October	89.4	0.933	0.998	0.931	92.0	0.750	0.991	0.744
November	81.2	0.857	0.996	0.853	84.2	0.682	0.985	0.670

The AUC values of the GAM for each month were all greater than 0.9 (Table 2). The deviance explained by the optimal GAM for each month also exceeded 70% (Table 2). However, the F1 and kappa scores of the BRT model were slightly higher overall than those for the GAM. Figure A4 shows the Q-Q plots of residuals from the GAM for each month from May to December.

3.6. The Relative Influence of Spatial and Environmental Variables

As shown in Figure 7, spatial variables have a significant effect on the fishing effort (FE). Among all the variables, longitude, distance from shore, and latitude rank first, second, and third, respectively. The impact of marine environmental variables on FE is nearly half as significant as that of longitude. These results indicate that spatial variables are the primary factors that influence the FE. Among all the marine environmental variables, chlorophyll (Chla0) and temperature at 300 m depth (T300) were the main factors affecting the FE, with chlorophyll having the strongest influence, second only to latitude. The remaining marine environmental variables have no significant differences in their impacts on the FE, with average influence values not exceeding 6. As shown in Figure 7, EKE has the least impact on the FE. Figure A5 shows the global sensitivity analysis results for the BRT model each month. It can be observed that the primary contributors to the model are lon, lat, and DSH, while chl, tem300, sst, sss, and do100 contribute to a lesser extent.

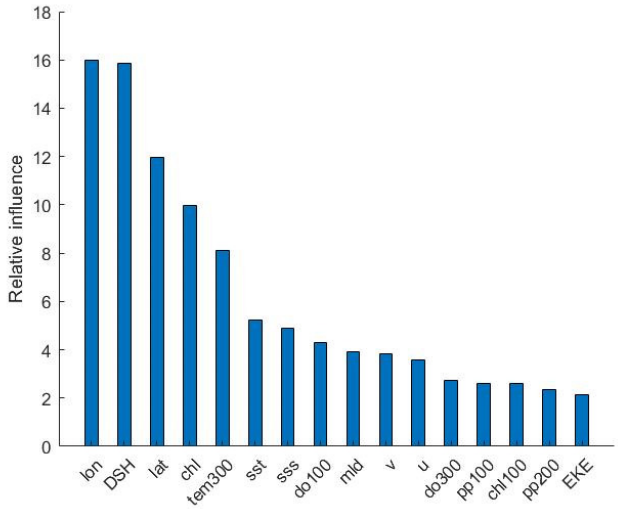

Figure 7. The relative influences of spatial and environmental variables on the FE.

3.7. Appropriate Ranges for the Environmental Variables

Figure A2a–g illustrates the relative impacts of the top three environmental variables on FE for each month. Although the influence of certain key variables fluctuates across months, their suitable ranges show minimal seasonal variation, as seen with T0 and T300. In general, the optimal temperature range for T0 remains around 12~20 °C, and for T300, it is approximately 3~6 °C. The appropriate ranges for other significant environmental variables influencing fishing efforts each month are provided in Table A2.

3.8. Extraction of the Potential Distributions of Light Purse Seine Vessels

We used the BRT model to predict the potential distributions of Chinese mainland light purse seine vessels in the Northwest Pacific for the year 2022. Figure 8 shows both the predicted potential FE distribution and the actual FE distributions of these vessels. The colored background represents the model's predicted potential FE distribution, whereas the white triangles represent the actual FE distribution. The predicted and actual FE distributions are generally similar.

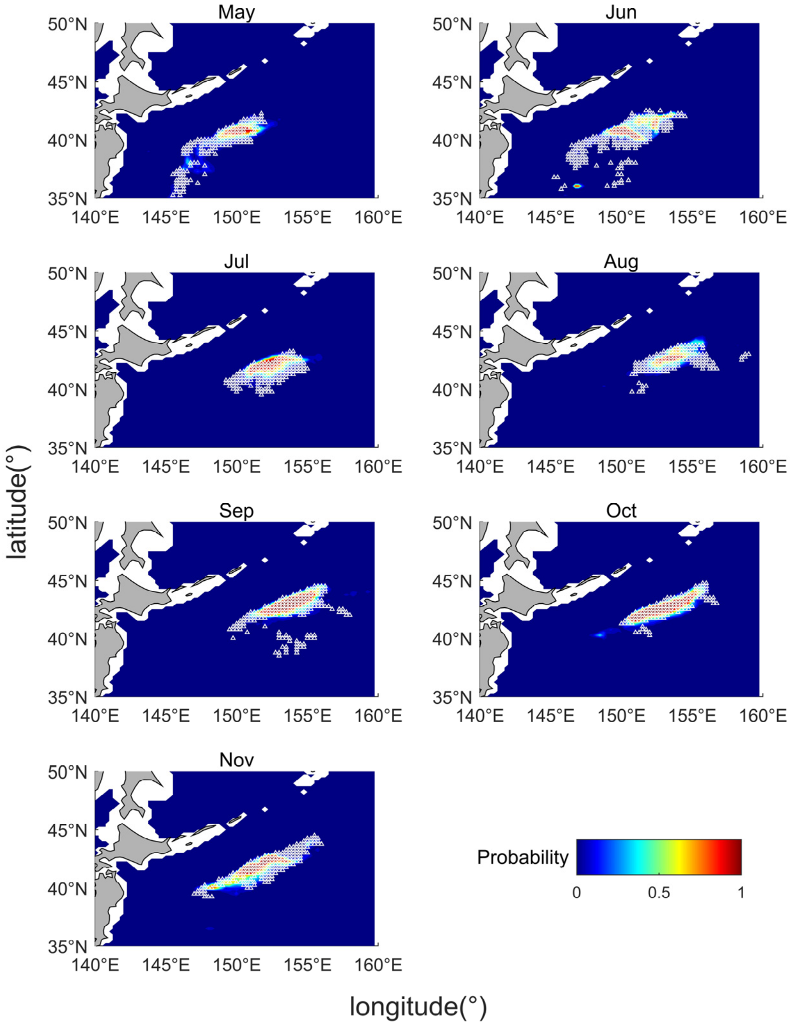

Figure 8. The potential activity distributions of Chinese mainland light seine vessels in the Northwest Pacific for 2022 compared with the actual distributions.

4. Discussion

4.1. Spatiotemporal Distribution of Light Purse Seine Fishing Activities

The results indicate that the primary fishing areas for light purse seine vessels from the Chinese mainland are located near Japan's exclusive economic zone, with fishing activities being highly concentrated (Figure 2). The temporal distribution of fishing activities is relatively even from May to November each year (Figure 3). This pattern may be related to the spatiotemporal distribution of the target species in the region and to fishing management practices. Fishermen are likely to choose to operate during the most promising fishing seasons (or months) and in the most productive areas to balance costs.

4.2. Accuracy of the BRT Model

The BRT model, a tree-based ensemble learning method, provides benefits such as preventing overfitting [22]. The AUC values of the selected BRT models from May to November are 0.996, 0.991, 0.995, 0.999, 0.995, 0.998, and 0.996, respectively (Table 2). The explained deviation for the optimal BRT models in each month exceeds 50%, indicating that the model is stable [12]. Although the GAM also has AUC values above 0.9, its F1 and kappa scores are lower (Table 2). Therefore, the BRT model might be better suited for predicting fishing efforts compared to the GAM. However, the BRT model also has certain limitations, as it assumes that the effects of environmental variables on species distributions remain consistent, implying spatial smoothness between these variables; this spatial smoothness may not always hold at the large spatial scale of marine ecosystems. Consequently, the BRT model does not fully capture spatial heterogeneity regarding how environmental variables affect fishing vessel operations.

Zhao et al. noted that light purse seine vessels in the Northwest Pacific typically fish chub mackerel from May to November each year [28]. It is reasonable for the AUCs in May to be slightly lower than those in other months, as fishing operations might not be fully underway when the vessels first arrive at the fishing grounds. Yukami et al. reported that chub mackerel gradually migrated northeast to approximately 170° E before August of each year and then started migrating southwest to areas east of 150° starting in September [29]. The lower AUCs in September than in August and October may be due to vessels trailing the migrating mackerels and the fact that fishing activities are not driven completely by the parameters we chose. The fishing grounds are located near the exclusive economic zone, which restricts vessels from fully following the mackerel's migration routes. Table 2 shows that the BRT model has high F1 scores, deviance explained, and kappa scores each month, indicating that our model is effective in classifying the fishing effort.

Additionally, we used the BRT model to predict the potential distribution of light purse seine vessels from the Chinese mainland in the Northwest Pacific for the year 2022 and compared these with the actual FE distribution. As shown in the results (Figure 8), the predicted potential fishing grounds are generally consistent with the actual FE distribution in terms of spatial patterns. This finding indicates that our model has a certain predictive ability and that the selected environmental variables are representative to some extent.

4.3. Influence of Spatial Variables on FE

In this paper, we analyzed light purse seine vessels located in the Northwest Pacific within the range of 35–50° N, 140° E–160° W for the years from 2020 to 2022. The Kuroshio current converges with the Oyashio current in this region [30]. The convergence of the Kuroshio and Oyashio currents is rich in nutrients, creating a favorable growth environment for marine organisms [31]. Chub mackerel gather in this region during the fishing season [32]. Therefore, it has become an important fishing ground for chub mackerel, resulting in a significant distribution of light purse seine vessels from the Chinese mainland within the study area.

As shown in Figure 8, the influence of longitude on the fishing effort (FE) is significantly greater than that of latitude. Yukami et al. noted that the longitudinal variations in chub mackerel are more pronounced than their latitudinal variations [29], which is consistent with the findings of this study. As shown in Figure A2a–g, the changes in the spatial distributions of the light purse seine vessels from the Chinese mainland are reflected primarily in the gradual northeastward and southwestward shifts between June and July and between August and September. Chub mackerel first move northeastward to feed and spawn and then move southwestward, and the shifting pattern of their aggregation area is related to the migratory habits of the species. There is a high degree of similarity between these movements and the seasonal shifts of the fleet. The influence of the distance from shore is evident in the fact that the light purse seine vessels from the Chinese mainland primarily operate outside the boundary of Japan's exclusive economic zone (EEZ), with the vessel density increasing as the EEZ boundary is approached. Therefore, as shown in Figure 2A, the shorter the distance from the shore, the greater its impact on the FE. As shown in Figure A5a–g, DSH, lon, and lat are the main contributors to the model output variance. Additionally, the contribution of lon and lat to the model output variance varies significantly across months, which aligns with the results obtained from the BRT model. The contribution of these variables to the model variance exhibits a clear seasonal pattern.

4.4. Influence of Marine Environmental Variables on the FE

The fishing fleet tracks the migration and habitat locations of fish. Therefore, the temporal and spatial changes in the fishing fleet reflect the spatiotemporal dynamics of fishery resources and are also a response to environmental changes. The chub mackerel exhibits distinct depth distributions and vertical movement patterns [17], indicating that marine environmental factors at different depths significantly impact the fishing activities of light purse seine vessels. Wang et al. reported that in the Northwest Pacific, chub mackerel often aggregate in areas with depths ranging from 50 to 100 m and significant temperature changes [33]. Therefore, examining the effects of marine environmental variables at different depths on chub mackerel fishing efforts is essential for achieving more reliable and robust research outcomes. The BRT model applied in this paper yielded strong training results, demonstrating its ability to effectively capture the relationship between the spatiotemporal dynamics of light purse seine vessels and environmental changes.

Numerous studies have demonstrated that sea temperatures are a key ecological influence in determining the distribution of chub mackerel fishery resources and the identification of possible fishing grounds. Dickson et al. (2002) reported that temperature directly impacts the swimming speed of chub mackerel [34]. Li et al. reported that the closer the water temperature is to 20 °C for juvenile chub mackerel, the more favorable it is for the subsequent growth and survival of adult fish [35]. Many experts and scholars have used fishery data to study the optimal sea temperature range for the survival of chub mackerel, which is between 10 °C and 22 °C [36]. The BRT model results show that the favorable fishing temperature range for T0 is between 12 °C and 20 °C, aligning with previously mentioned conclusions. Additionally, the average relative influence of T300 on FE from May to November is around 8.1% (Figure 7). This phenomenon suggests that deep-sea water temperatures have a significant effect on the activities of light purse seine fleets. The favorable range of T300 for FE is between 3 °C and 6 °C.

The influence of S0 on FE is 4.8% (Figure 7). Kitano et al. (2018) suggested that chub mackerel grow faster under low salinity conditions [37]. Michitaka et al. reported that the movement direction of chub mackerel fishing grounds aligns with the movement direction of the high-salinity Tsushima warm current [38]. Notably, the importance of S0 is more pronounced in July and November than in the other months (Figure A3c,f). The primary spawning period of chub mackerel is from January to June. In July, when chub mackerel undergo feeding migrations, they follow high-salinity water masses, which makes salinity a significant factor. In November, as chub mackerel begin migrating to their spawning grounds, salinity likely becomes important as they search for suitable spawning sites.

Chlorophyll-a has a significant effect on the FE, with the BRT model in this study showing that chlorophyll-a affects the FE by 10.0% (Figure 7). Dai et al. suggested that chlorophyll-a influences the migration routes of chub mackerel, with variations in chlorophyll-a within the distribution range of chub mackerel across different months, and these variations exhibit seasonal differences. Moreover, differences in chlorophyll-a can lead to local aggregations of chub mackerel, such as in the Kuroshio-Oyashio Extension area [39]. Chlorophyll contents are considered an indicator of primary productivity in marine ecosystems. Guan's study on the relationship between chub mackerel stock and net primary productivity revealed that the relationship between chub mackerel stocks and chlorophyll-a is not linear but rather parabolic. This finding indicates that an increase in chlorophyll-a within a certain range increases chub mackerel stocks, but beyond that range, further increases in chlorophyll-a may actually inhibit the expansion of stocks [40]. This finding aligns with the results shown in Figure A2a,d–g, where the fitness curve of Chla0 presents a parabolic shape.

The FE is also influenced by dissolved oxygen. The BRT model results in this study show that the impacts of DO100 and DO300 on the FE are less significant, with relative influences of 4.3% and 2.7%, respectively (Figure 7). Barange et al. noted that chub mackerel typically inhabit water layers at depths of 50–100 m, where the dissolved oxygen levels are relatively low [41]. This finding is consistent with the results of this study, where the lower oxygen levels in deeper waters led chub mackerel to swim toward areas with higher dissolved oxygen levels. Consequently, the influence of dissolved oxygen at a depth of 100 m is greater than that at 300 m, and the relative influence of dissolved oxygen at 100 m is lower than that of other variables such as temperature, salinity, and chlorophyll-a.

The mixed layer depth and primary productivity have a minimal impact on the FE, likely because the primary productivity metrics used in this study apply to depths of 100 m and 200 m, whereas chub mackerel primarily feed in the shallower layers [17]. Chlorophyll-a is considered an indicator of primary productivity in marine ecosystems. However, sea surface primary productivity, which has a more significant influence, was removed from the analysis because of its strong collinearity with sea surface chlorophyll-a.

As shown in Figure A5a–g, variables such as T0 and S0 exhibit a high contribution to the model output variance, consistent with the relative influence results from the BRT model. However, there is a notable difference in the case of chlorophyll-a. While chlorophyll-a is relatively important in the BRT model, its contribution is lower in the Sobol indices, particularly its first-order Sobol index. This may indicate that it primarily influences the model's output variance through interactions with other variables rather than through a direct effect.

5. Conclusions

Based on AIS data, this study applies the BRT model to establish nonlinear relationships between fishing intensity and predictor variables and explores the ecological and environmental drivers behind the spatial distribution of the light purse seine vessels from the Chinese mainland in the Northwest Pacific. This research identifies the key influencing factors, predicts the spatiotemporal distributions of fishing intensity, and reveals significant seasonal preferences for different marine environments in various months. Additionally, the influence of environmental data obtained from the model aligns with existing research. The suitable sea surface temperature range is between 12 °C and 20 °C, while salinity primarily affects the growth rate of chub mackerel, which in turn influences its spawning migration routes. The impact of chlorophyll-a concentration exhibits an inverted parabolic trend. These factors are key drivers in altering the migration routes of chub mackerel, with chlorophyll-a identified as the primary influencing factor. The predicted potential fishing effort closely matches the observed data, providing valuable information to support fisheries resource management and planning.

Author Contributions: Conceptualization, L.W. and S.Y.; methodology, L.W., S.Y. and L.Y.; software, L.W., S.Y. and L.Y.; formal analysis, S.Y., L.Y., F.W. and J.S.; data curation, L.W., S.Y. and F.W.; writing—original draft preparation, L.W.; writing—review and editing, S.Y.; validation, S.Z., K.J. and Z.W.; visualization, W.Z., F.W. and Y.D.; supervision, W.F.; project administration, S.Y., L.Y. and W.F. All authors have read and agreed to the published version of the manuscript.

Funding: This research was funded by the National Key R&D Program of China (2023YFD2401303) and the Laoshan Laboratory (LSKJ202201801, LSKJ202201804).

Institutional Review Board Statement: Not applicable.

Informed Consent Statement: Not applicable.

Data Availability Statement: Publicly available datasets of vessel numbers and marine environment were analyzed in this study. The vessel number data can be found here: https://globalfishingwatch.org/, accessed on 8 May 2023. The marine environment data can be found here: https://data.marine.copernicus.eu/products, accessed on 8 May 2023.

Acknowledgments: The authors of this research would like to thank all the researchers who contributed to the research process during our study. The authors are grateful to the Global Fishing Watch for the GFW website. We acknowledge the use of oceanic parameter data from the Copernicus Marine Environment Monitoring Service. Thanks for the data provided by Global Fishing Watch Data.

Conflicts of Interest: The authors declare no conflicts of interest.

Appendix A

Table A1. Environmental data.

Variable Explained	Abbreviation	Unit	Original Resolution
Water Temperature (0 m)	T_0	°C	0.083°
Water Temperature (100 m)	T_{100}	°C	0.083°
Water Temperature (200 m)	T_{200}	°C	0.083°
Water Temperature (300 m)	T_{300}	°C	0.083°
Chlorophyll-a (0 m)	$Chla_0$	$mg \cdot m^{-3}$	0.25°
Chlorophyll-a (100 m)	$Chla_{100}$	$mg \cdot m^{-3}$	0.25°
Chlorophyll-a (200 m)	$Chla_{200}$	$mg \cdot m^{-3}$	0.25°
Chlorophyll-a (300 m)	$Chla_{300}$	$mg \cdot m^{-3}$	0.25°
Salinity (0 m)	S_0	10^{-3} (dimensionless)	0.083°
Salinity (100 m)	S_{100}	10^{-3}	0.083°
Salinity (200 m)	S_{200}	10^{-3}	0.083°
Salinity (300 m)	S_{300}	10^{-3}	0.083°
Primary production (0 m)	PP_0	$mg \cdot m^{-3} \cdot day^{-1}$	0.25°
Primary production (100 m)	PP_{100}	$mg \cdot m^{-3} \cdot day^{-1}$	0.25°
Primary production (200 m)	PP_{200}	$mg \cdot m^{-3} \cdot day^{-1}$	0.25°
Primary production (300 m)	PP_{300}	$mg \cdot m^{-3} \cdot day^{-1}$	0.25°
Dissolved oxygen (0 m)	DO_0	$mmol \cdot m^{-3}$	0.25°
Dissolved oxygen (100 m)	DO_{100}	$mmol \cdot m^{-3}$	0.25°
Dissolved oxygen (200 m)	DO_{200}	$mmol \cdot m^{-3}$	0.25°
Dissolved oxygen (300 m)	DO_{300}	$mmol \cdot m^{-3}$	0.25°
Sea surface high	SSH	m	0.083°
Mixed layer depth	MLD	m	0.083°
Eastward velocity	u	$m \cdot s^{-1}$	0.083°
Northward velocity	v	$m \cdot s^{-1}$	0.083°

Table A2. The suitable interval of different variables for fishing effort.

Month	Variable	Suitable Interval
May	$Chla_0$	0.8~1.3 $mg \cdot m^{-3}$
	DO_{300}	140~160 $mmol \cdot m^{-3}$
	MLD	20~30 m
June	MLD	12~21 m
	T_0	10~19 °C
	T_{300}	3~6 °C
July	T_0	15~20 °C
	S_0	32~33 × 10^{-3}
	T_{300}	3~7 °C
August	T_0	16~22 °C
	$Chla_0$	0.4~0.7 $mg \cdot m^{-3}$
	T_{300}	3~7 °C
September	T_0	16~22 °C
	$Chla_0$	0.1~0.5 $mg \cdot m^{-3}$
	PP_{100}	0.1~0.3 $mg \cdot m^{-3} \cdot day^{-1}$
October	$Chla_0$	0.2~0.6 $mg \cdot m^{-3}$
	T_0	12~20 °C
	MLD	20~40 m
November	S_0	32~33 × 10^{-3}
	T_0	11~17 °C
	$Chla_0$	0.4~0.5 $mg \cdot m^{-3}$

Table A3. Statistical characteristics of GAM model for variables.

Month	Variable	edf	Chi.sq	*p*-Value	AIC
May	lon	4.0435	100.935	$<2 \times 10^{-16}$	640.08
	DSH	4.0968	105.034	$<2 \times 10^{-16}$	
	sst	4.5649	23.704	1.54×10^{-5}	
	sss	6.0870	21.285	0.000430	
	mld	1.5644	14.150	0.000148	
	u	1.0444	18.917	9.26×10^{-7}	
	v	3.5949	16.754	0.000206	
	EKE	0.9649	3.038	0.020464	
	chl	7.0584	57.477	$<2 \times 10^{-16}$	
	T300	2.3187	30.946	$<2 \times 10^{-16}$	
	chl	1.0543	22.019	1.40×10^{-6}	
	pp100	3.0744	16.727	0.000224	
June	lon	7.051	59.58	$<2 \times 10^{-16}$	1022.01
	lat	5.020	44.71	$<2 \times 10^{-16}$	
	DSH	8.168	44.82	$<2 \times 10^{-16}$	
	sst	6.786	28.37	3.31×10^{-5}	
	sss	4.880	34.24	1.16×10^{-6}	
	mld	6.340	75.44	$<2 \times 10^{-16}$	
	v	4.965	45.06	$<2 \times 10^{-16}$	
	EKE	6.143	30.61	4.50×10^{-7}	
	chl	5.182	29.02	5.98×10^{-6}	
	T300	8.732	50.22	$<2 \times 10^{-16}$	
	do300	6.880	18.28	0.005567	
	do100	6.229	29.49	8.87×10^{-6}	
	pp100	4.419	19.14	0.000182	
	pp200	4.833	12.20	0.008950	
July	lon	3.889	39.69	$<2 \times 10^{-16}$	502.24
	lat	6.021	50.22	$<2 \times 10^{-16}$	
	DSH	4.604	52.01	$<2 \times 10^{-16}$	
	sst	4.578	48.36	$<2 \times 10^{-16}$	
	sss	4.087	26.35	6.06×10^{-6}	
	mld	5.778	21.49	0.00044	
	chl	7.994	40.60	$<2 \times 10^{-16}$	
	T300	7.222	28.28	5.11×10^{-5}	
	chl300	3.241	37.92	$<2 \times 10^{-16}$	
	pp200	4.896	27.45	1.29×10^{-5}	
August	lon	7.590	48.19	$<2 \times 10^{-16}$	398.10
	lat	6.142	47.89	$<2 \times 10^{-16}$	
	DSH	6.129	34.80	$<2 \times 10^{-16}$	
	sst	6.590	37.42	$<2 \times 10^{-16}$	
	sss	6.954	31.44	1.79×10^{-5}	
	mld	7.431	27.26	0.000256	
	u	1.098	18.71	9.26×10^{-6}	
	EKE	3.779	14.92	0.002285	
	chl	4.924	13.07	0.013921	
	chl100	7.072	22.40	0.001579	
	do300	8.456	33.23	3.79×10^{-5}	
	do100	6.102	26.92	5.51×10^{-5}	

Table A3. *Cont.*

Month	Variable	edf	Chi.sq	p-Value	AIC
September	lon	5.838	53.72	$<2 \times 10^{-16}$	708.10
	lat	7.921	85.02	$<2 \times 10^{-16}$	
	DSH	7.931	81.44	$<2 \times 10^{-16}$	
	sst	5.171	46.14	$<2 \times 10^{-16}$	
	sss	4.206	13.39	0.00349	
	mld	6.639	37.65	$<2 \times 10^{-16}$	
	v	1.835	28.81	$<2 \times 10^{-16}$	
	chl	1.515	30.36	$<2 \times 10^{-16}$	
	T300	1.253	15.80	3.75×10^{-5}	
	chl100	6.036	39.54	$<2 \times 10^{-16}$	
	do300	7.949	45.20	$<2 \times 10^{-16}$	
	do100	6.132	56.25	$<2 \times 10^{-16}$	
	pp100	1.240	21.35	1.93×10^{-6}	
October	lon	6.828	37.48	$<2 \times 10^{-16}$	351.85
	lat	5.921	33.02	3.57×10^{-6}	
	DSH	5.465	65.71	$<2 \times 10^{-16}$	
	sst	6.143	29.91	5.54×10^{-6}	
	u	8.234	24.40	0.001296	
	chl	4.812	52.44	$<2 \times 10^{-16}$	
	do300	3.830	17.10	0.000270	
	do100	4.662	21.23	7.37×10^{-5}	
	pp100	3.801	18.70	0.000202	
November	lon	5.924	53.400	$<2 \times 10^{-16}$	570.88
	lat	6.195	20.624	0.001383	
	DSH	4.211	73.082	$<2 \times 10^{-16}$	
	sst	4.324	30.184	1.92×10^{-6}	
	sss	6.737	32.909	$<2 \times 10^{-16}$	
	mld	2.020	5.898	0.029518	
	u	3.809	32.809	$<2 \times 10^{-16}$	
	do300	4.857	10.736	0.027994	
	do100	3.983	36.614	$<2 \times 10^{-16}$	
	pp200	2.631	14.908	0.000261	

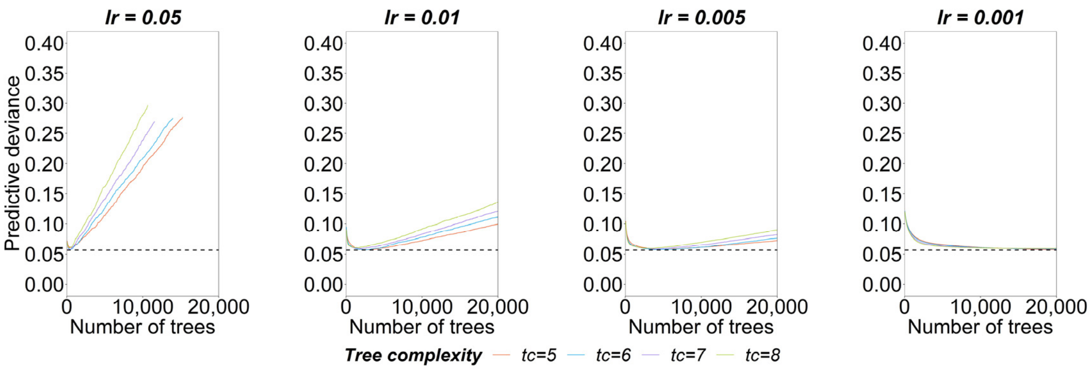

(**a**) May

Figure A1. *Cont.*

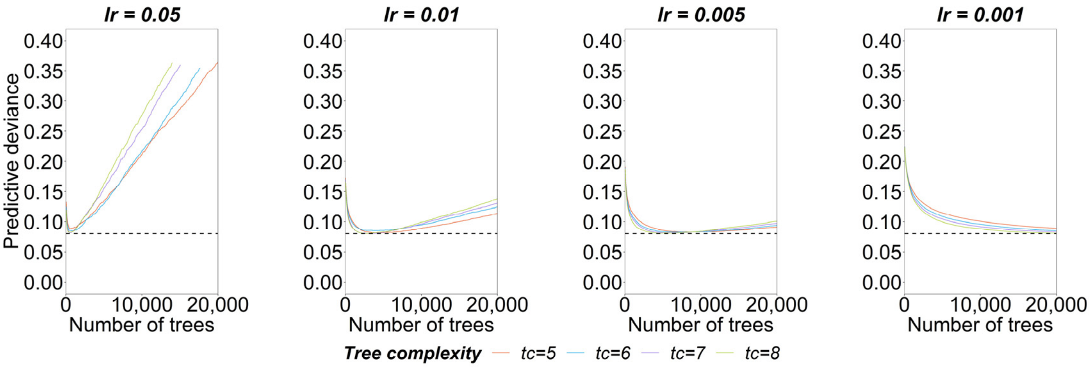

(**b**) June

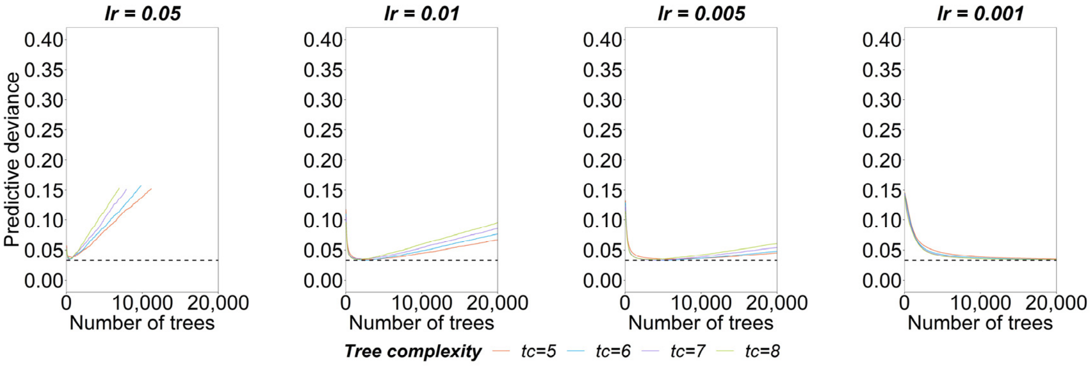

(**c**) July

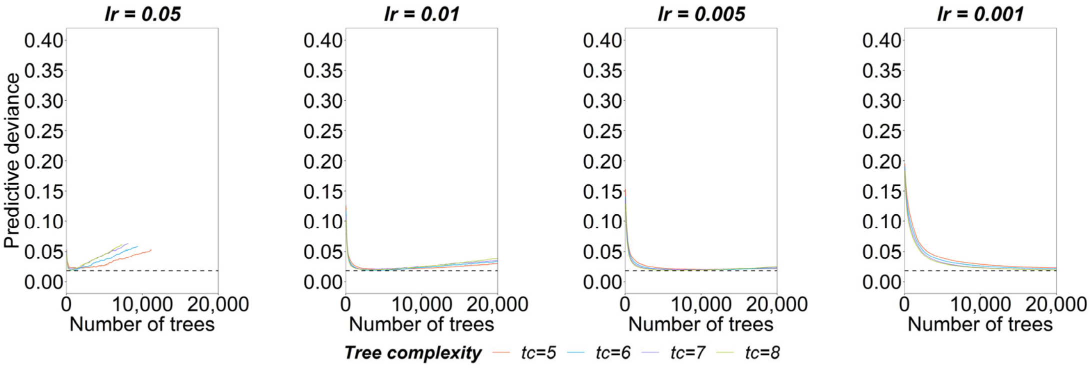

(**d**) August

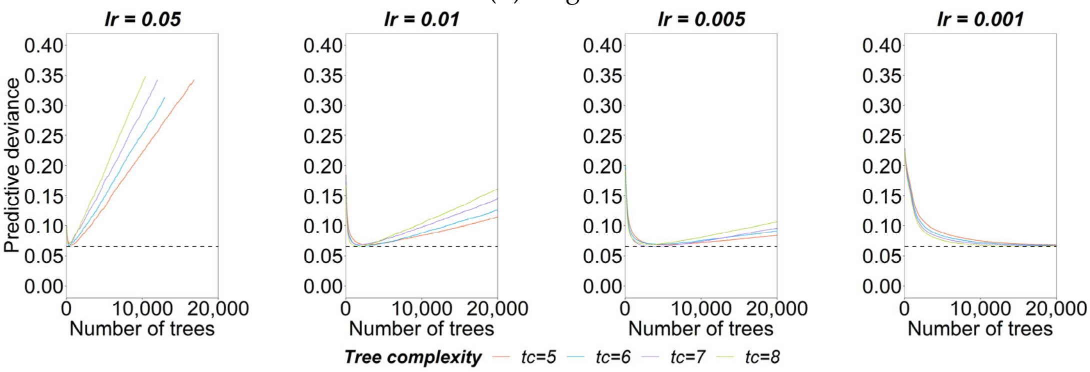

(**e**) September

Figure A1. *Cont*.

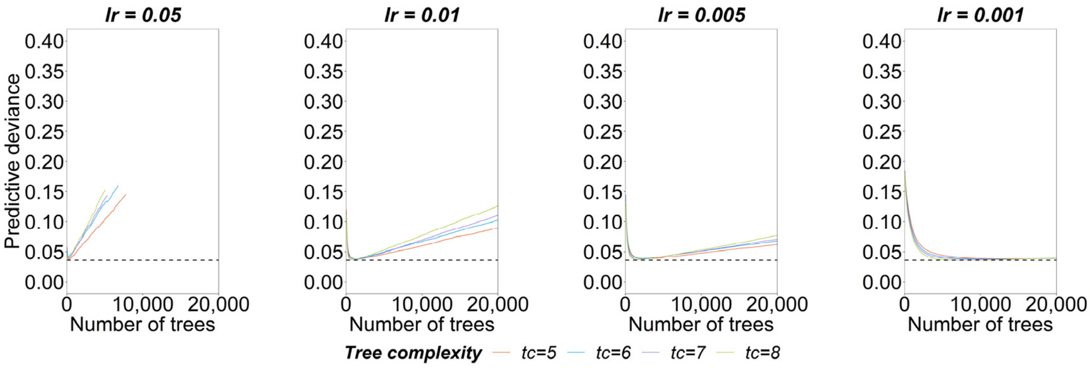

(**f**) October

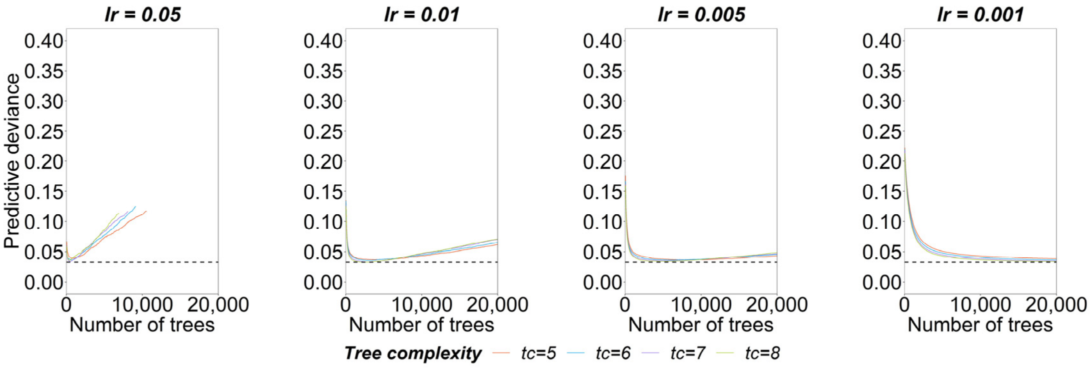

(**g**) November

Figure A1. The relationship between predictive deviance and number of trees for BRT model under different learning rate and tree complexity in each month.

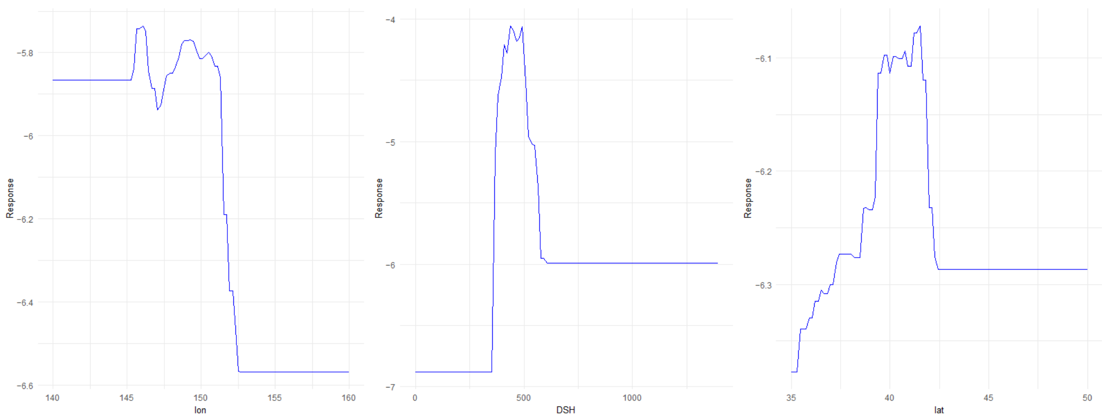

(**a**) May

Figure A2. *Cont.*

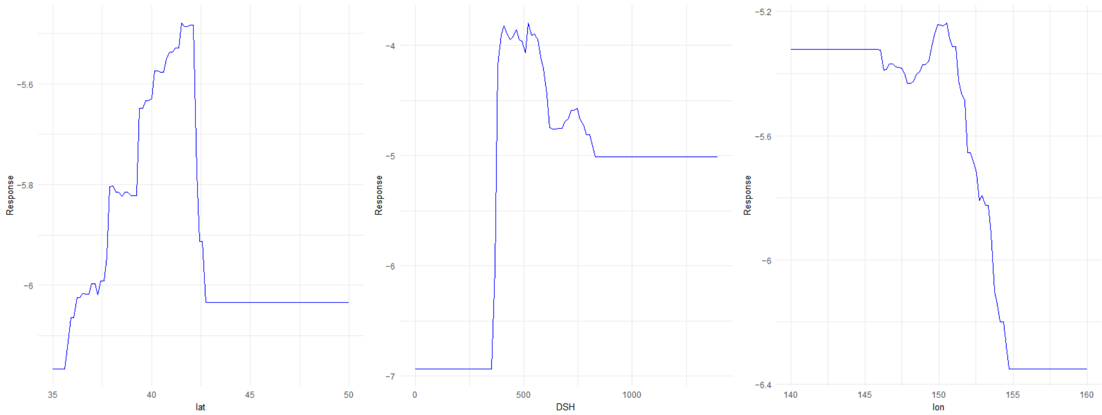

(**b**) June

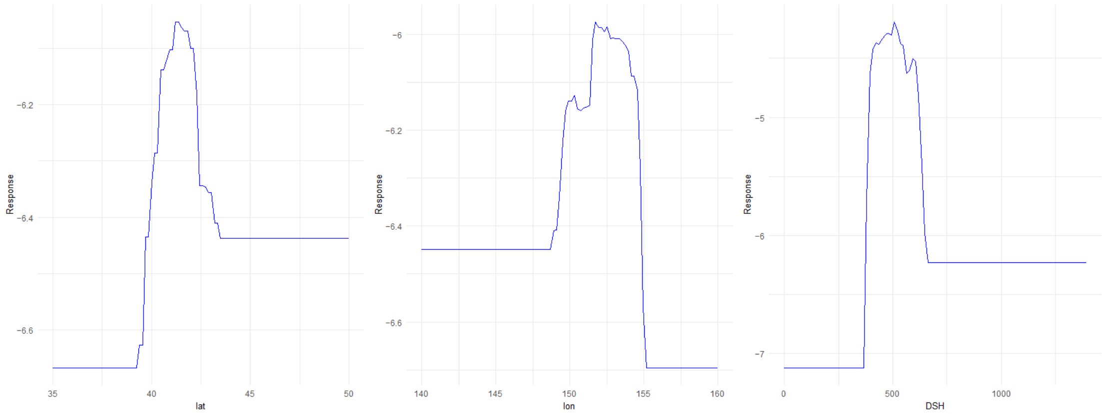

(**c**) July

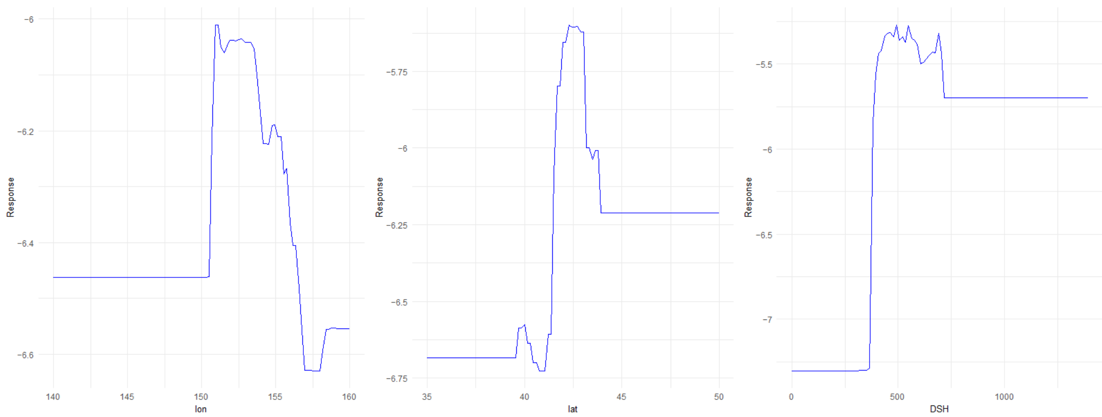

(**d**) August

Figure A2. *Cont*.

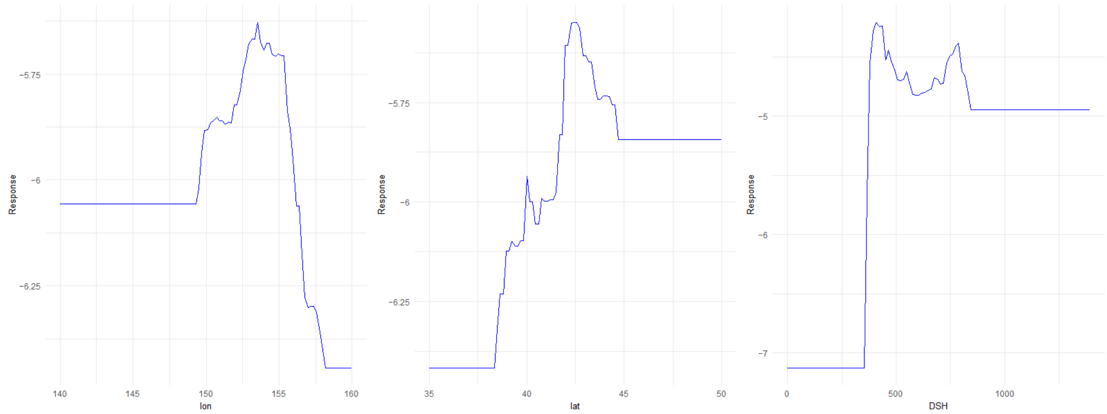

(**e**) September

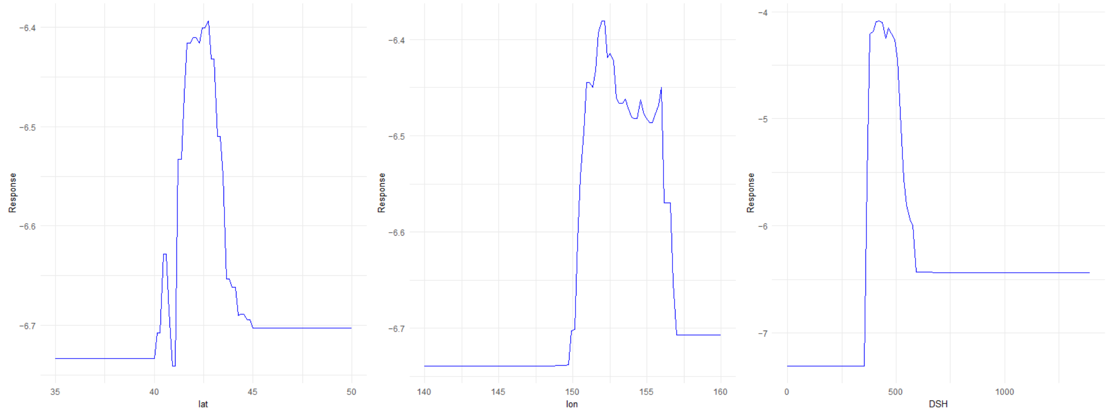

(**f**) October

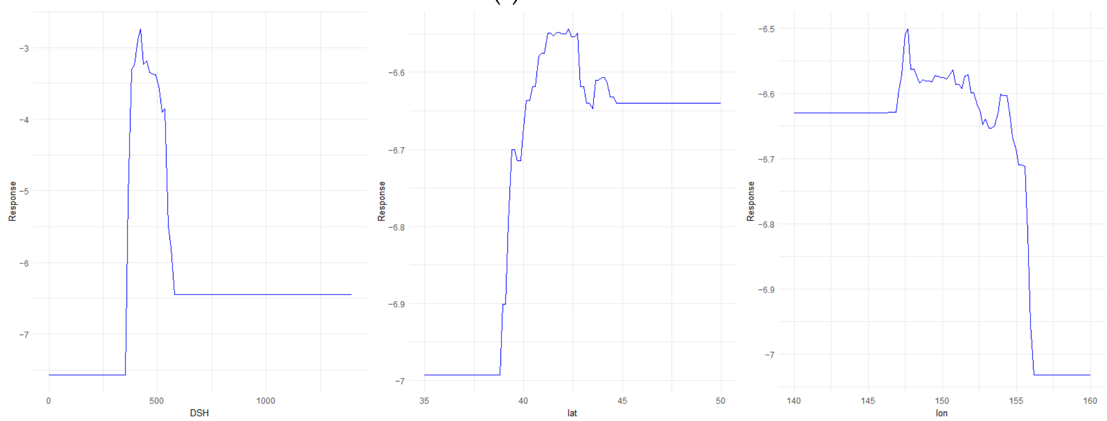

(**g**) November

Figure A2. Influence of latitude and longitude on FE in each month.

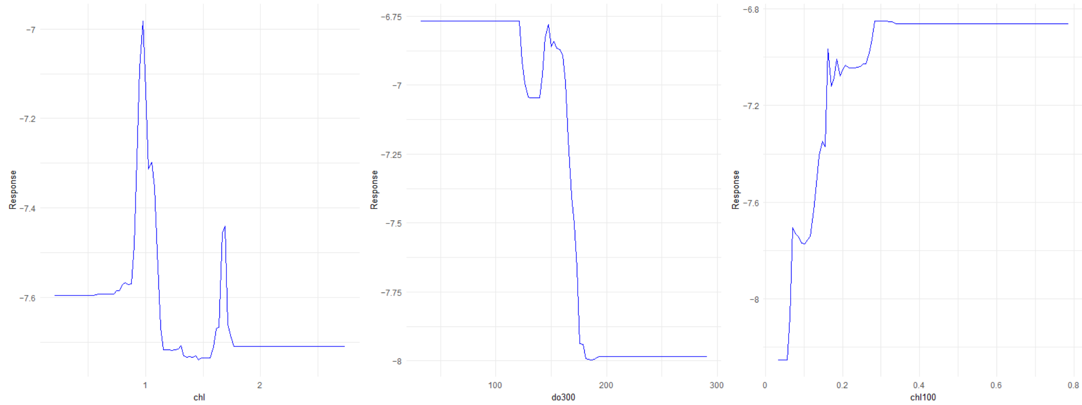

(**a**) May

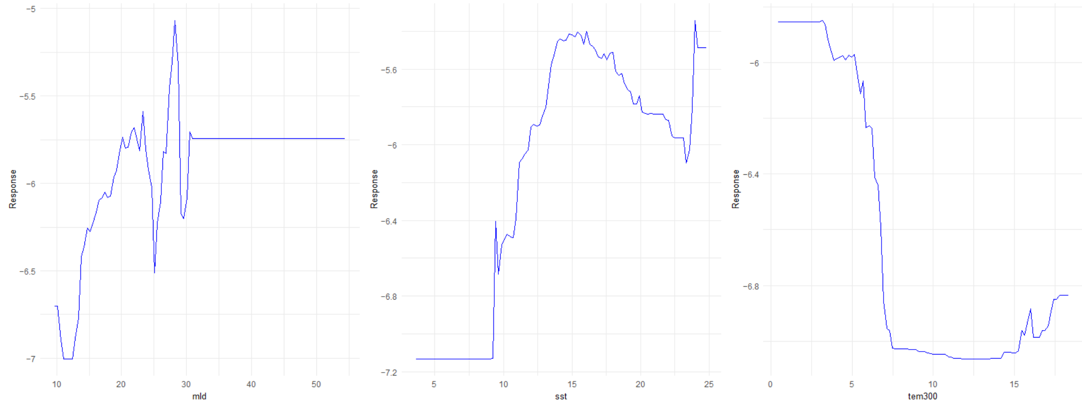

(**b**) June

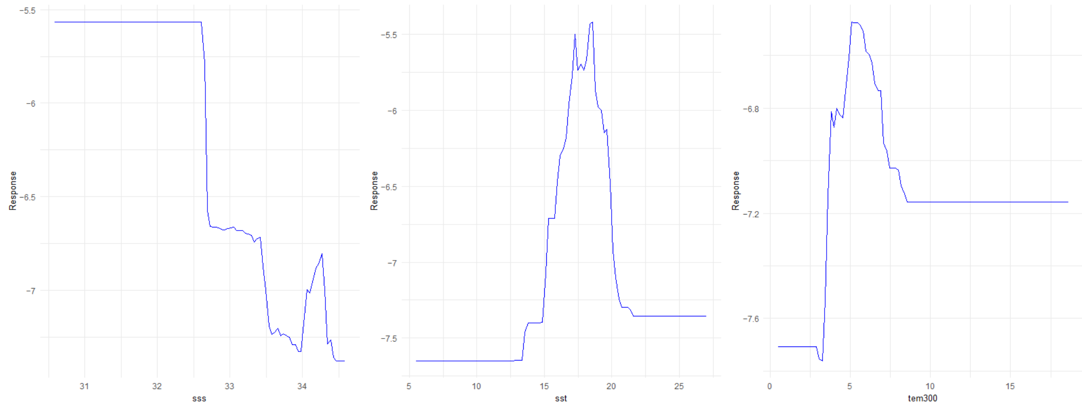

(**c**) July

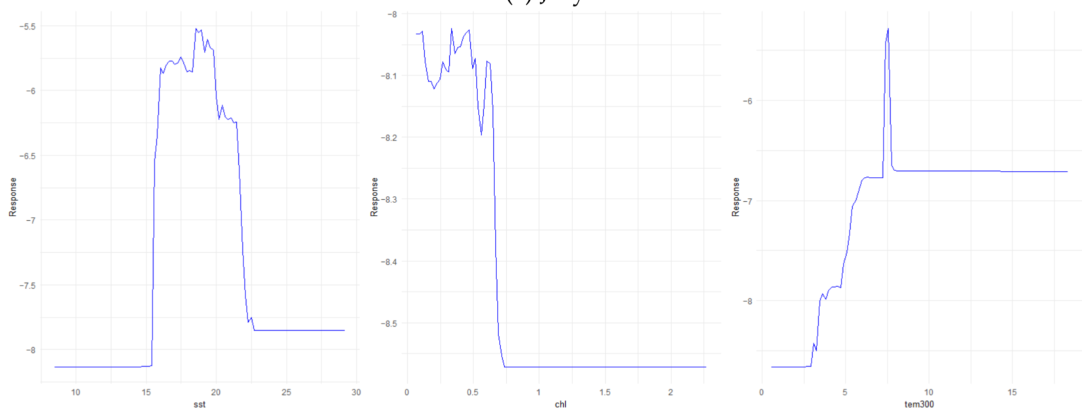

(**d**) August

Figure A3. *Cont*.

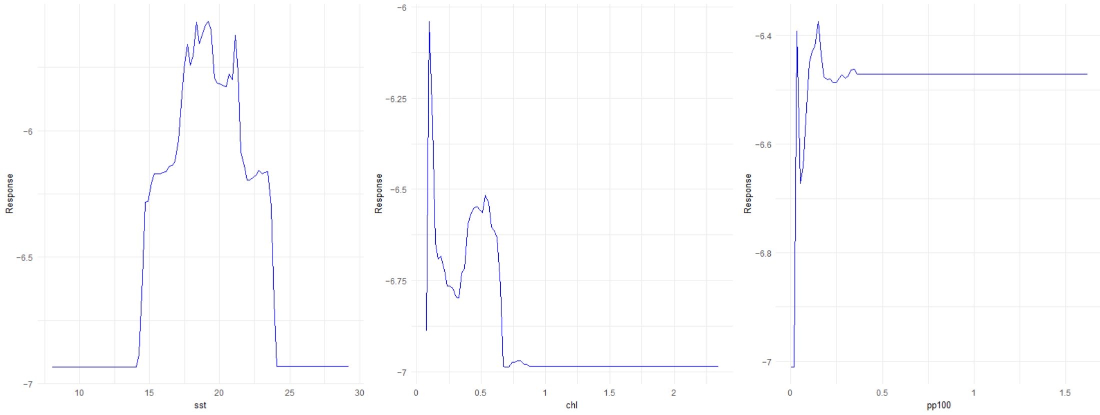

(**e**) September

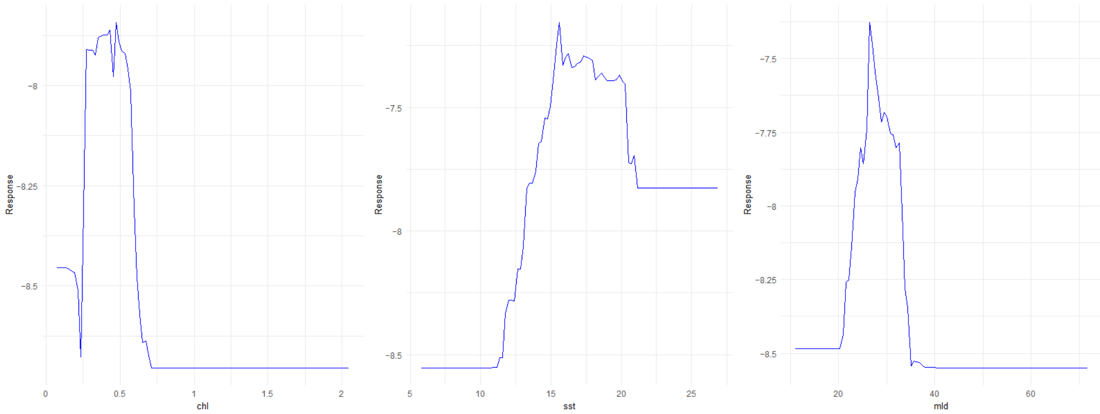

(**f**) October

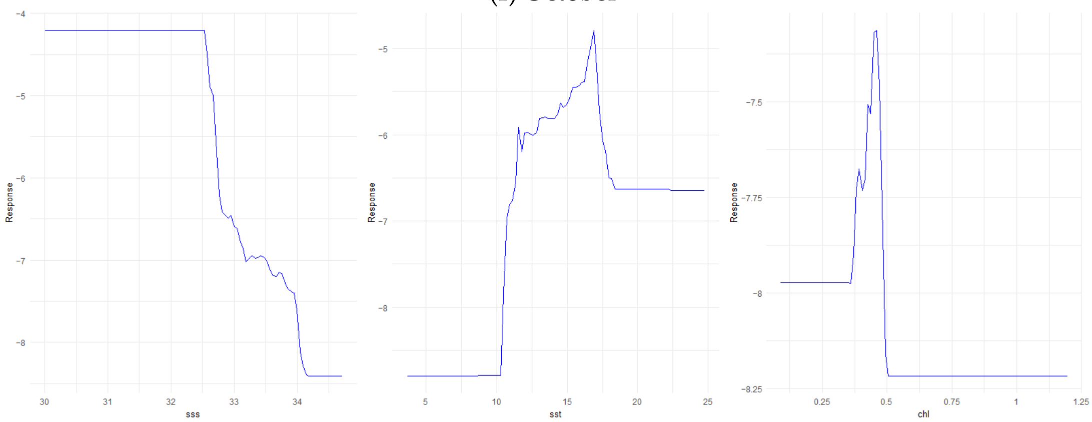

(**g**) November

Figure A3. Influence of important environmental variables on FE in each month.

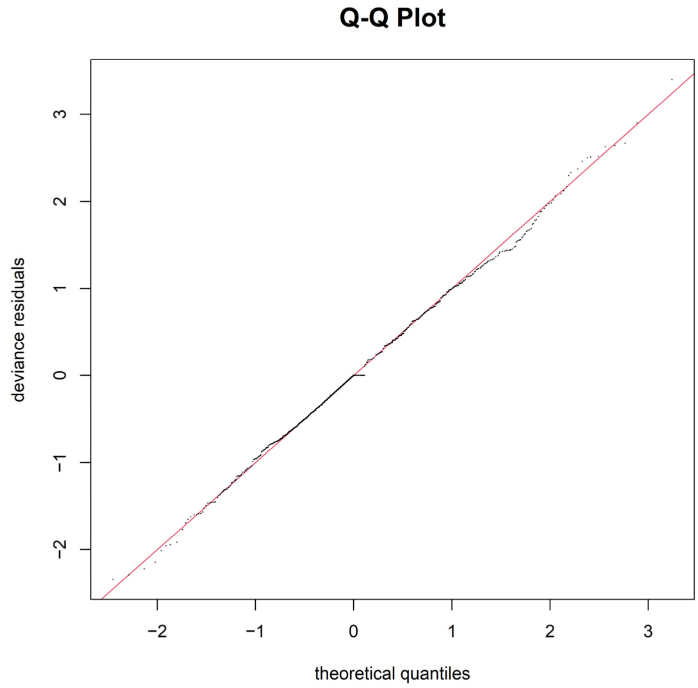

(**a**) May

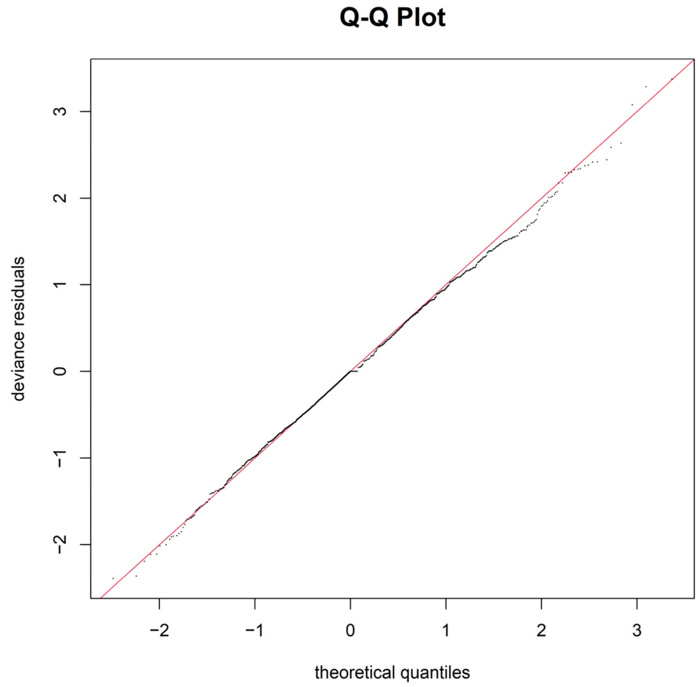

(**b**) June

Figure A4. *Cont*.

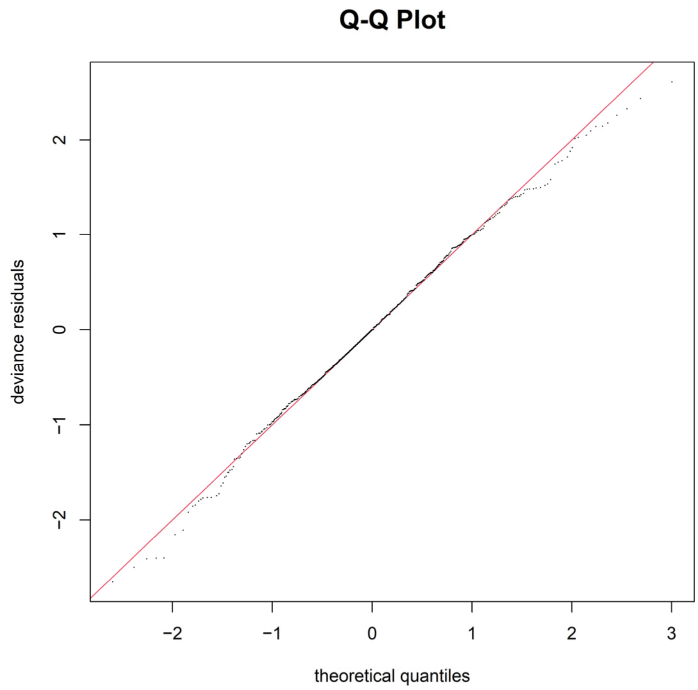

(**c**) July

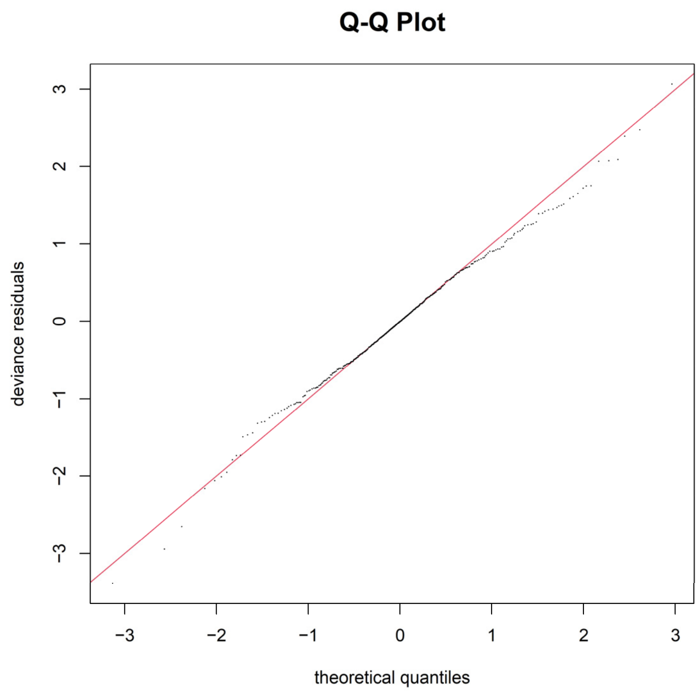

(**d**) August

Figure A4. *Cont*.

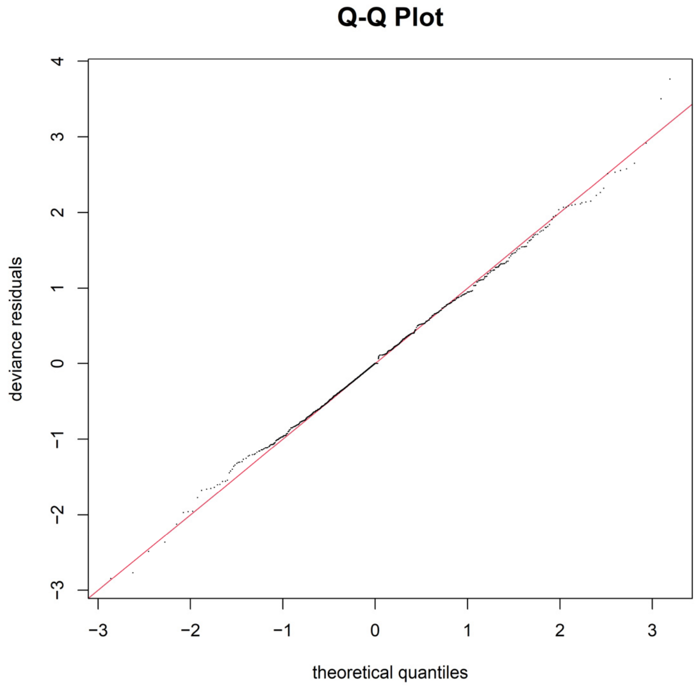

(**e**) September

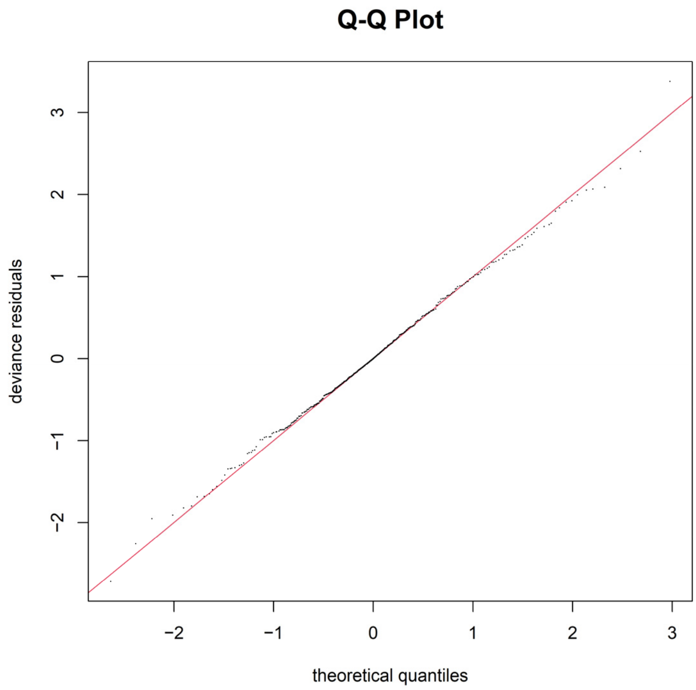

(**f**) October

Figure A4. *Cont.*

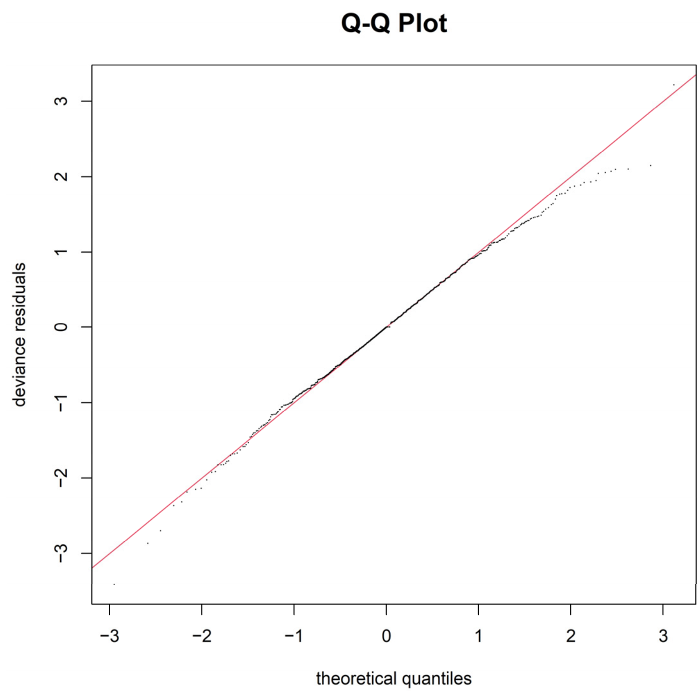

(**g**) November

Figure A4. Q-Q Plot for the GAM model in each month.

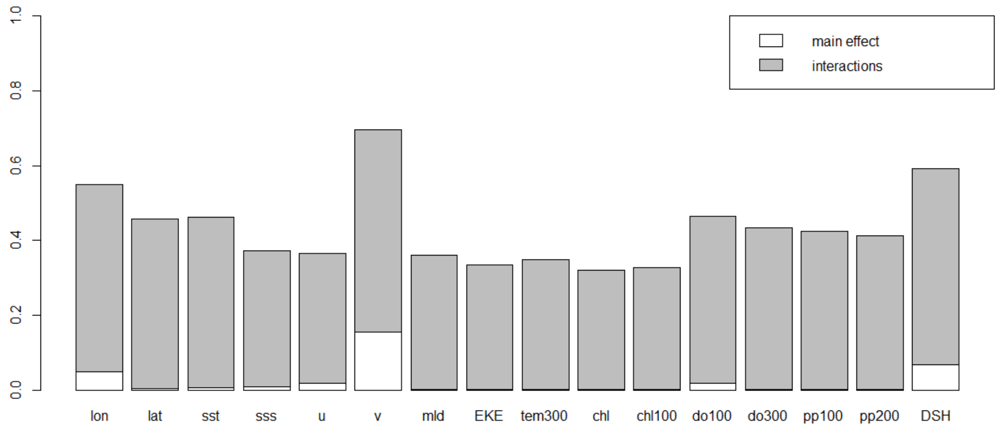

(**a**) May

Figure A5. *Cont.*

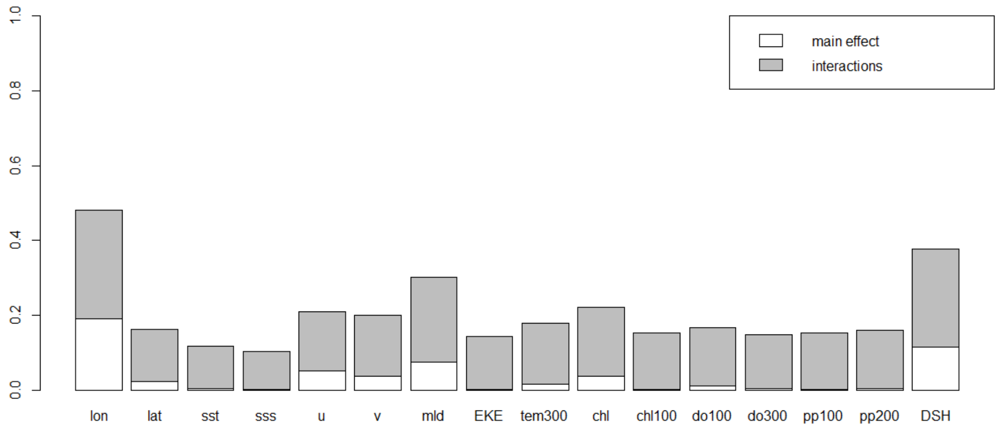

(**b**) June

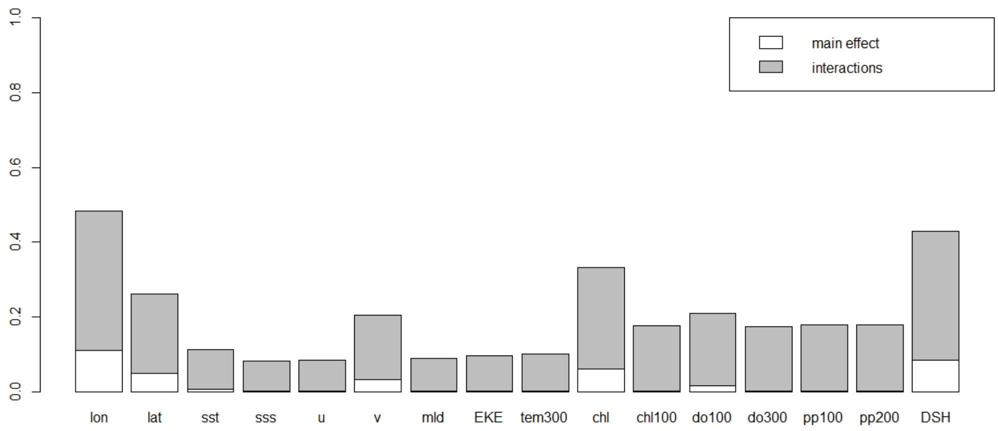

(**c**) July

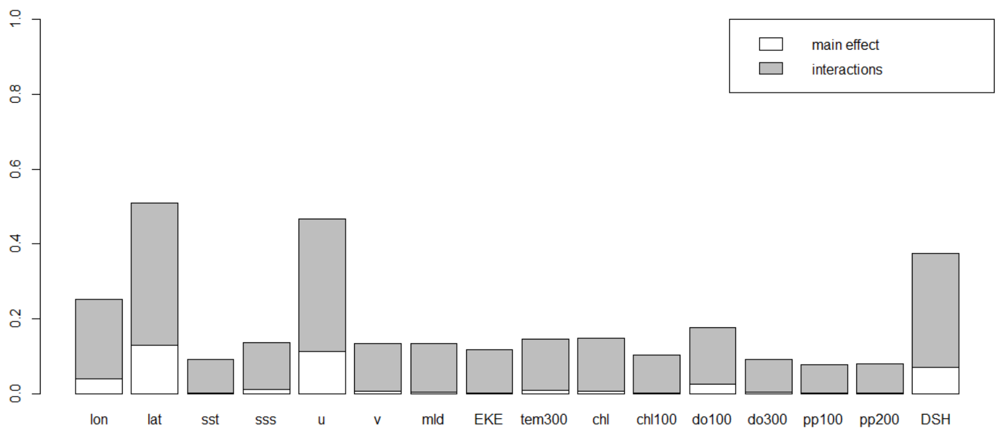

(**d**) August

Figure A5. *Cont.*

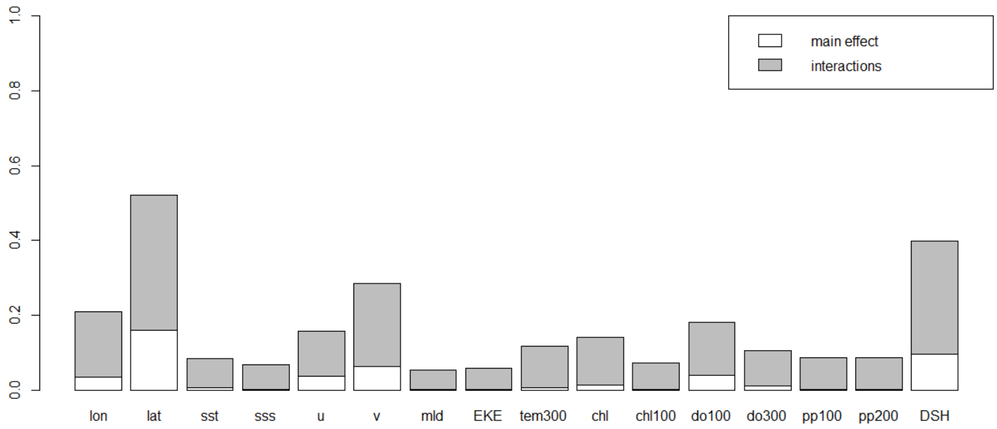

(**e**) September

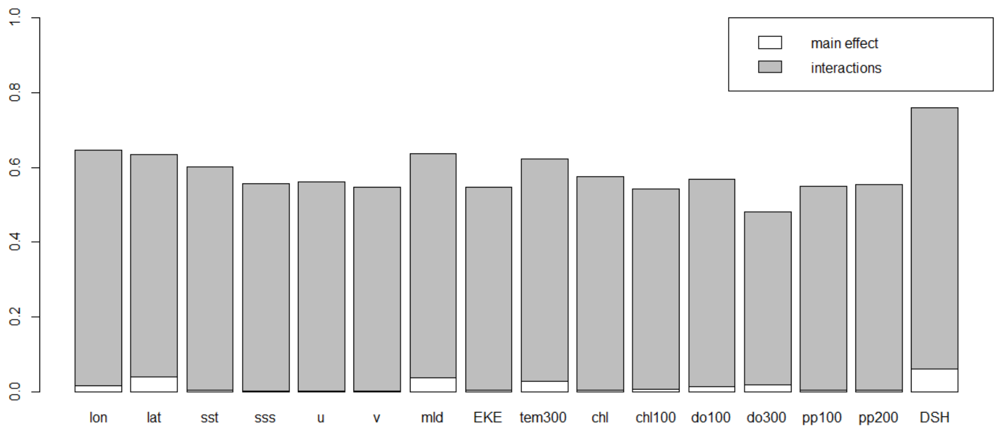

(**f**) October

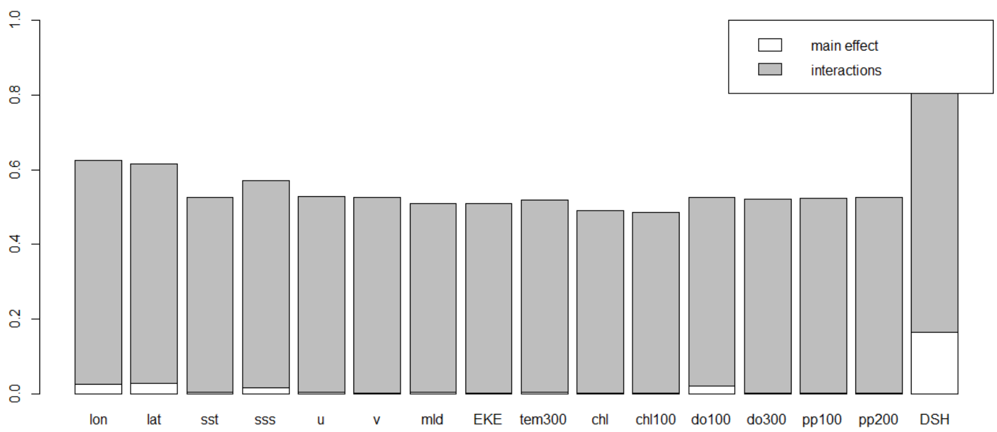

(**g**) November

Figure A5. Global Sensitivity Analysis Results.

References

1. Arthur, R.I.; Skerritt, D.J.; Schuhbauer, A.; Ebrahim, N.; Friend, R.M.; Sumaila, U.R. Small-scale fisheries and local food systems: Transformations, threats and opportunities. *Fish Fish.* **2022**, *23*, 109–124. [CrossRef]
2. Golden, C.D.; Allison, E.H.; Cheung, W.W.L.; Dey, M.M.; Halpern, B.S.; McCauley, D.J.; Smith, M.; Vaitla, B.; Zeller, D.; Myers, S.S. Nutrition: Fall in fish catch threatens human health. *Nature* **2016**, *534*, 317–320. [CrossRef] [PubMed]
3. Seto, K.L.; Miller, N.A.; Kroodsma, D.; Hanich, Q.; Miyahara, M.; Saito, R.; Boerder, K.; Tsuda, M.; Oozeki, Y.; Urrutia, S.O. Fishing through the cracks: The unregulated nature of global squid fisheries. *Sci Adv.* **2023**, *9*, eadd8125. [CrossRef] [PubMed]
4. Welch, H.; Clavelle, T.; White, T.D.; Cimino, M.A.; Van Osdel, J.; Hochberg, T.; Kroodsma, D.; Hazen, E.L. Hot spots of unseen fishing vessels. *Sci. Adv.* **2022**, *8*, 44. [CrossRef] [PubMed]
5. Soykan, C.U.; Eguchi, T.; Kohin, S.; Dewar, H. Prediction of fishing effort distributions using boosted regression trees. *Ecol. Appl.* **2014**, *24*, 71–83. [CrossRef]
6. Setiawati, M.D.; Sambah, A.B.; Miura, F.; Tanaka, T.; As-syakur, A.R. Characterization of bigeye tuna habitat in the Southern Waters off Java–Bali using remote sensing data. *Adv. Space Res.* **2015**, *55*, 732–746. [CrossRef]
7. Hashimoto, M.; Nishijima, S.; Yukami, R.; Watanabe, C.; Kamimura, Y.; Furuichi, S.; Ichinokawa, M.; Okamura, H. Spatiotemporal dynamics of the Pacific chub mackerel revealed by standardized abundance indices. *Fish. Res.* **2019**, *219*, 105315. [CrossRef]
8. Shi, Y.; Zhang, H.; Ma, Q.; Yang, C.; Zhao, G. Standardized CPUE of Chub Mackerel (Scomber japonicas) Caught by the China's Lighting Purse Seine Fishery up to 2019. North Pacific Fisheries Commission: Tokyo, Japan, 2021.
9. Cimino, M.A.; Anderson, M.; Schramek, T.; Merrifield, S.; Terrill, E.J. Towards a Fishing Pressure Prediction System for a Western Pacific EEZ. *Sci. Rep.* **2019**, *9*, 461. [CrossRef]
10. Crespo, G.O.; Dunn, D.C.; Reygondeau, G.; Boerder, K.; Worm, B.; Cheung, W.; Tittensor, D.P.; Halpin, P.N. The environmental niche of the global high seas pelagic longline fleet. *Sci Adv* **2018**, *4*, eaat3681. [CrossRef]
11. Debrah, E.A.; Wiafe, G.; Agyekum, K.A.; Aheto, D.W. An Assessment of the Potential for Mapping Fishing Zones off the Coast of Ghana using Ocean Forecast Data and Vessel Movement. *West Afr. J. Appl. Ecol.* **2018**, *26*, 26–43.
12. Wang, Y.B.; Wang, Y. Estimating catches with automatic identification system (AIS) data: A case study of single otter trawl in Zhoushan fishing ground, China. *Iran. J. Fish. Sci.* **2016**, *15*, 75–90. [CrossRef]
13. Wan, L.; Cheng, T.; Fan, W.; Shi, Y.; Zhang, H.; Zhang, S.; Yu, L.; Dai, Y.; Yang, S. Spatial information extraction of fishing grounds for light purse seine vessels in the Northwest Pacific Ocean based on AIS data. *Heliyon* **2024**, *10*, e28953. [CrossRef] [PubMed]
14. Chen, X.; Li, G.; Feng, B.; Tian, S. Habitat suitability index of Chub mackerel (*Scomber japonicus*) from July to September in the East China Sea. *J. Oceanogr.* **2009**, *65*, 93–102. [CrossRef]
15. Lee, D.; Son, S.; Kim, W.; Park, J.M.; Joo, H.; Lee, S.H. Spatio-Temporal Variability of the Habitat Suitability Index for Chub Mackerel (*Scomber Japonicus*) in the East/Japan Sea and the South Sea of South Korea. *Remote Sens.* **2018**, *10*, 938. [CrossRef]
16. Yu, W.; Guo, A.; Zhang, Y.; Chen, X.; Qian, W.; Li, Y. Climate-induced habitat suitability variations of chub mackerel *Scomber japonicus* in the East China Sea. *Fish. Res.* **2018**, *207*, 63–73. [CrossRef]
17. Yasuda, T.; Kinoshita, J.; Niino, Y.; Okuyama, J. Vertical migration patterns linked to body and environmental temperatures in chub mackerel. *Prog. Oceanogr.* **2023**, *213*, 103017. [CrossRef]
18. Belkin, I.M.; O'Reilly, J.E. An algorithm for oceanic front detection in chlorophyll and SST satellite imagery. *J. Mar. Syst.* **2009**, *78*, 319–326. [CrossRef]
19. Scharffenberg, M.G.; Stammer, D. Seasonal variations of the large-scale geostrophic flow field and eddy kinetic energy inferred from the TOPEX/Poseidon and Jason-1 tandem mission data. *J. Geophys. Res. Ocean.* **2010**, *115*, C02008. [CrossRef]
20. Salmerón Gómez, R.; Rodríguez Sánchez, A.; García, C.G.; García Pérez, J. The VIF and MSE in raise regression. *Mathematics* **2020**, *8*, 605. [CrossRef]
21. Tibshirani, R.; Hastie, T.; Friedman, J.H. *The Elements of Statistical Learning: Data Mining, Inference, and Prediction*; with 200 Full-Color Illustrations; Springer: New York, NY, USA, 2001.
22. Elith, J.; Leathwick, J.R.; Hastie, T. A working guide to boosted regression trees. *J. Anim. Ecol.* **2008**, *77*, 802–813. [CrossRef]
23. Leathwick, J.R.; Elith, J.; Francis, M.P.; Hastie, T.; Taylor, P. Variation in demersal fish species richness in the oceans surrounding New Zealand: An analysis using boosted regression trees. *Mar. Ecol. Prog. Ser.* **2006**, *321*, 267–281. [CrossRef]
24. Kamaruzzaman, Y.N.; Mustapha, M.A.; Ghaffar, M.A. Determination of Fishing Grounds Distribution of the Indian Mackerel in Malaysia's Exclusive Economic Zone Off South China Sea Using Boosted Regression Trees Model. *Thalass.: Int. J. Mar. Sci.* **2021**, *37*, 147–161. [CrossRef]
25. Swets, J.A. Measuring the accuracy of diagnostic systems. *Science* **1988**, *240*, 1285–1293. [CrossRef]
26. Derville, S.; Constantine, R.; Baker, C.S.; Oremus, M.; Torres, L.G. Environmental correlates of nearshore habitat distribution by the Critically Endangered Māui dolphin. *Mar. Ecol. Prog. Ser.* **2016**, *551*, 261–275. [CrossRef]
27. Yu, H.; Cooper, A.R.; Infante, D.M. Improving species distribution model predictive accuracy using species abundance: Application with boosted regression trees. *Ecol. Modell.* **2020**, *432*, 109202. [CrossRef]
28. Zhao, G.; Shi, Y.; Fan, W.; Cui, X.; Tang, F. Study on main catch composition and fishing ground change of light purse seine in Northwest Pacific. *South China Fish. Sci.* **2022**, *18*, 33–42. [CrossRef]
29. Yukami, R.; Ohshimo, S.; Yoda, M.; Hiyama, Y. Estimation of the spawning grounds of chub mackerel *Scomber japonicus* and spotted mackerel *Scomber australasicus* in the East China Sea based on catch statistics and biometric data. *Fish. Sci.* **2009**, *75*, 167–174. [CrossRef]

30. Talley, L.D. Distribution and Formation of North Pacific Intermediate Water. *J. Phys. Oceanogr.* **1993**, *23*, 517–537. [CrossRef]
31. Fan, W.; Wu, Y.; Cui, X. The study on fishing ground of neon flying squid, *Ommastrephes bartrami*, and ocean environment based on remote sensing data in the Northwest Pacific Ocean. *Chin. J. Oceanol. Limnol.* **2009**, *27*, 408–414. [CrossRef]
32. Furuichi, S.; Kamimura, Y.; Yukami, R. Length–length and Length–weight Relationships for Four Dominant Small Pelagic Fishes in the Kuroshio–Oyashio Current System. *Thalass. Int. J. Mar. Sci.* **2021**, *37*, 651–657. [CrossRef]
33. Liangming, W.; Yuan, L.; Ran, Z.; YongJun, T.; Jun, Z.; Longshan, L. Relationship between the resource distribution of *Scomber japonicus* and seawater temperature vertical structure of Northwestern Pacific Ocean. *Period. Ocean. Univ. China* **2019**, *49*, 29–38.
34. Dickson, K.A.; Donley, J.M.; Sepulveda, C.; Bhoopat, L. Effects of temperature on sustained swimming performance and swimming kinematics of the chub mackerel *Scomber japonicus*. *J. Exp. Biol.* **2002**, *205*, 969–980. [CrossRef] [PubMed]
35. Yuesong, L.; Lingzhi, P.; Liping, Y.; Xinjun, C. Individual-based model study on the fishing ground of chub mackerel in the East China Sea. *Haiyang Xuebao* **2014**, *36*, 67–74. (In Japanese)
36. Perrotta, R.G.; Viñas, M.D.; Hernandez, D.R.; Tringali, L. Temperature conditions in the Argentine chub mackerel (*Scomber japonicus*) fishing ground: Implications for fishery management. *Fish. Oceanogr.* **2001**, *10*, 275–283. [CrossRef]
37. Kitano, H.; Nagano, N.; Sakaguchi, K.; Matsuyama, M. Effect of low salinity on the expression profile of Na^+/K^+-ATPase and the growth of juvenile chub mackerel (*Scomber japonicus* Houttuyn). *Aquac. Res.* **2018**, *49*, 352–358. [CrossRef]
38. Michitake, U. Japan relationship between sea conditions and fishing conditions in the East Japan Sea. *Tsushima Warm Stream Dev. Surv. Rep.* **1958**, *1*, 501–539.
39. Dai, S.W.; Tang, F.H.; Fan, W.; Zhang, H.; Cui, X.S.; Guo, G.G. Distribution of resource and environment characteristics of fishing ground of *Scomber japonicas* in the North Pacific high seas. *Mar. Fish.* **2017**, *39*, 372–382. [CrossRef]
40. Wenjian, G. Study on the dynamics of biomass of chub mackerel based on ocean net primary production in southern East China Sea. *Acta Oceanol. Sin.* **2013**, *5*, 121–127. [CrossRef]
41. Barange, M.; Bernal, M.; Cergole, M.C.; Cubillos, L.A.; Daskalov, G.M.; de Moor, C.L.; De Oliveira, J.A.A.; Dickey-Collas, M.; Gaughan, D.J.; Hill, K.; et al. Current trends in the assessment and management of stocks. In *Climate Change and Small Pelagic Fish*; Checkley, D., Alheit, J., Oozeki, Y., Roy, C., Eds.; Cambridge University Press: Cambridge, UK, 2009.